Thesis for the degree of Doctor of Philosophy in Natural Science,
Specialization in Chemistry

Atmospheric Chemistry of Volatile Organic Compounds: Oxidation products, Mechanisms and Secondary Organic Aerosol Formation

Julia Hammes

UNIVERSITY OF GOTHENBURG

Department of Chemistry and Molecular Biology
University of Gothenburg
412 96 Göteborg
Sweden

Doctoral thesis submitted for fulfilment of the requirements for the degree of Doctor of Philosophy in Chemistry

February 2019

Atmospheric Chemistry of Volatile Organic Compounds:
Oxidation products, Mechanisms and Secondary Organic Aerosol Formation

©Julia Hammes, 2019

Cover picture: Atmospheric chemistry and aerosol formation over Hong Kong forest
Photo: Christian Mark Salvador

Atmospheric Science
Department of Chemistry and Molecular Biology
University of Gothenburg
412 96 Göteborg
Sweden

Printed by BrandFactory AB
BrandFactory AB Kållered, Sweden

ISBN: 978-91-7833-069-0 (PRINT)
ISBN: 978-91-7833-070-6 (PDF)

Abstract

The results from this work are a piece in understanding the complex puzzle of atmospheric aerosol formation. Secondary organic aerosol (SOA) formed by the oxidation of volatile organic compounds (VOC) in the atmosphere is a key component of air pollution with a strong negative impact on human health and influence on climate, but its formation is poorly understood. Because air pollution and climate change are major challenges facing modern societies, there is a clear need to better understand atmospheric SOA formation. SOA formation can be estimated from distributions of potential oxidation products, but such estimates are only as useful as the underlying chemical mechanisms and physical properties on which they are based.

The work presented in this thesis was conducted to better characterize VOC oxidation products and the chemical mechanisms governing their formation. The SOA precursor compounds α-pinene and limonene (representing biogenic VOC) and 1,3,5-trimethylbenzene (TMB) (an anthropogenic VOC) were studied in the G-FROST and Go:PAM flow reactors to characterize their oxidation and the subsequent SOA-forming processes. Previously unknown compounds including dimer esters, carboxylic acids, nitrates and highly oxygenated molecules were identified using state-of-the-art mass spectrometric methods. These oxidation products were shown to be important SOA contributors and explicit mechanisms for their formation were proposed. Some of the identified compounds were suggested to be of extremely low volatility and thus important for new particle formation. Oxidation of TMB under conditions representative of urban environments reduced particle formation potential; this effect was attributed to the disruption of RO_2 auto-oxidation cycles by NO_x and subsequent nitrate formation at the expense of highly oxygenated molecules. During the course of this work, an automated algorithm was developed to extract compound-specific volatility data from FIGAERO thermograms.

The scientific understanding of SOA formation would be greatly improved by a detailed knowledge of the products of VOC oxidation, the mechanisms by which they are formed, and their vapour pressures, all of which this work aims to contribute to.

Keywords: SOA, VOC, anthropogenic, biogenic, FIGAERO, CIMS, HOMs, ELVOCs, atmospheric oxidation, chemical mechanism, NO_x, limonene, α-pinene, TMB, ozone, nitrate, OH, radical chemistry, RO_2, G-FROST, GO:PAM

Sammanfattning

Målet med arbetet som presenteras i denna avhandling är att bättre förstå det komplexa pusslet som atmosfärisk aerosolbildning utgör. I fokus är en viktig luftföroreningskomponent, den sekundära organiska aerosolen (SOA), som bildas genom atmosfärisk oxidation av flyktiga organiska ämnen och som kan ha negativa hälsoeffekter. SOA har även en avkylande effekt på klimatet och kan därmed dölja en del av den globala uppvärmningen orsakad av växthusgaser. SOAs betydelse för klimatet samt dess negativa påverkan på luftkvalitén utgör ett starkt skäl till att förbättra förståelsen av atmosfärisk SOA-bildning. SOA-bildning kan generellt uppskattas utifrån framtagna oxidationsproduktfördelningar men för att kunna göra tillförlitliga uppskattningar måste man har en hög kvalitet på de underliggande kemiska mekanismerna samt en bra beskrivning av de ingående ämnenas fysikaliska egenskaper.

Innehållet i denna avhandling bidrar till en ökad förståelsen för de kemiska mekanismer som kan leda till SOA bildning och oxidationsprodukter kopplade till dessa mekanismer. Specifikt har oxidations- och SOA-bildningen från två biogena (α–pinen och limonen) och ett antropogent (1,3,5-trimetylbenzen, TMB) ämne studerats i flödesreaktorerna G-FROST och Go:PAM. Flera tidigare okända oxidationsprodukter har identifierats med hjälp av toppmoderna masspektrometriska metoder. Dessa nya ämnen inkluderar dimerestrar, karboxylsyror, nitrater och starkt oxygenerade molekyler. Samtliga dessa oxidationsprodukter är viktiga för förståelsen av SOA-bildning och explicita bildningsmekanismer har kunnat föreslås. Vissa av de identifierade föreningarna har extremt låg flyktighet och är därmed av stort intresse för att förstå den atmosfäriska bildningen av nya partiklar. Under detta arbete har även en del metodutveckling gjorts. Till exempel har en ny algoritm utvecklats för att automatisera extrahering av ämnespecifika flyktighetsdata för organiska ämnen uppmätta med en metod som innebär termisk desoption-analys med högupplöst mass-spektrometri.

Keywords: SOA, VOC, antropogen, biogen, FIGAERO, CIMS, HOMs, ELVOCs, atmosfärisk oxidation, kemiska mekanismer, NO_x, limonen, α-pinen, TMB, ozon, nitrat, OH, radikal kemi, RO_2, G-FROST, Go:PAM

List of Publications

My thesis is based on the following appended papers, referred to in the text by their Roman numerals.

I **High-molecular weight dimer esters are major products in aerosols from α-pinene ozonolysis and the boreal forest**
Kristensen, K., Watne, Å. K., Hammes, J., Lutz, A., Petäjä, T., Hallquist, M., Bilde, M. and Glasius, M.; Environ. Sci. Technol. Lett., 3 (8), 280–285, 2016; DOI: 10.1021/acs.estlett.6b00152

II **Characterization of organic nitrate constituents of secondary organic aerosol (SOA) from nitrate-radical-initiated oxidation of limonene using High-Resolution Chemical Ionization Mass Spectrometry**
Faxon, C., Hammes, J., Pathak, R. K., and Hallquist, M.; Atmos. Chem. Phys., 18, 5467-5481, 2018; DOI: 10.5194/acp-18-5467-2018

III **Carboxylic acids from limonene oxidation by ozone and OH radicals: Insights into mechanisms derived using a FIGAERO-CIMS**
Hammes, J., Lutz, A., Mentel, T., Faxon, C. and Hallquist, M.; Atmos. Chem. Phys. Discuss., in review, 2018; DOI: 10.5194/acp-2018-1004

IV **Effect of NOx on 1,3,5-trimethylbenzene (TMB) oxidation product distribution and particle formation**
Hammes, J., Tsiligiannis, E., Mentel, T. and Hallquist, M.;
Manuscript in preparation, 2018

V **A method for extracting calibrated volatility information from the FIGAERO-HR-ToF-CIMS and application to chamber and field work studies**
Bannan, T. J., Le Breton, M., Priestley, M., Worrall S. D., Bacak, A., Marsden, N., Hammes, J., Hallquist, M., Alfarra R., Krieger U. K., Reid, J., Jayne J., Gordon McFiggans, G., Hugh Coe, H., Percival, C. J. and Topping, D.;
Atmos. Meas. Tech. Discuss., in review, 2018; DOI: 10.5194/amt-2018-255

Statement of Contribution

I Julia Hammes (JH) performed all of the experiments using the G-FROST and PAM facilities in Gothenburg and extracted the aerosol samples. JH contributed to the analytical results and to writing the paper.

II JH contributed to planning and performing the experimental work and to writing the paper.

III JH had the main responsibility for designing the study, performing the experimental work and collecting data, analysing and interpreting the results and writing the paper.

IV JH had the main responsibility for designing the study, planning and performing the experimental work, analysing and interpreting the results and writing the paper.

V JH contributed to the analysis of GU-CIMS data and to writing the paper.

Contents

List of Figures

List of Tables

List of Schemes

List of Abbreviations

AVOC	Anthropogenic Volatile Organic Compound
BSQ	Big Segmented Quadrupole
BVOC	Biogenic Volatile Organic Compound
CCN	Cloud Condensation Nuclei
CDC	Collisional Dissociation Chamber
CI*	Excited Criegee Intermediate
CI	Criegee Intermediate
CPC	Condensation Particle Counter
DMA	Differential Mobility Analyser
ELVOC	Extremely Low Volatile Organic Compound
FIGAERO	Filter Inlet for GAses and AEROsols
G - FROST	Gothenburg Flow Reactor for Oxidation Studies at low Temperatures
Go:PAM	Gothenburg Potential Aerosol Mass Chamber
GUFIT	Gothenburg University FItting for Thermograms
HOMs	Highly Oxygenated Molecules
HR	High Resolution
IMR	Ion Molecule Reaction Chamber
IVOC	Intermediate Volatile Organic Compound
LVOC	Low Volatile Organic Compound

MCM	Master Chemical Mechanism
MW	Molecular Weight
NPF	New Particle Formation
ON	Organo Nitrate
PAN	Peroxy Acyl Nitrates
PFHA	Perfluorinated Heptanoic Acid, $C_7HF_{13}O_2$
POZ	Primary Ozonide
sCI	Stabilized Criegee Intermediate
SMPS	Scanning Mobility Particle Sizer
SOA	Secondary Organic Aerosol
SOZ	Secondary Ozonide
SSQ	Small Segmented RF - only Quadrupole
SVOC	Semi Volatile Organic Compound
TMB	1,3,5-trimethylbenzene, C_9H_{12}
ToF - CIMS	Time of Flight Chemical Ionization Mass Spectrometry
VHP	Vinyl Hydro Peroxide
VOC	Volatile Organic Compound
VP	saturation Vapor Pressure

Part I

Extended Summary

1

Our atmosphere and its pollutants

This chapter introduces the reader to our earth's atmosphere and its constituents. Air pollution and climate change are addressed and key suspects identified. Section 1.3 presents the aims of this PhD project and the research questions answered in this thesis. Finally, the structure of the thesis is outlined.

Contents

1.1 The earth's atmosphere

Life as we know it would not exist on earth without the atmosphere that surrounds it. It protects us from DNA-damaging ultraviolet solar radiation and creates the pressure that allows liquid water to exist on the earth's surface. Radiatively active gases (i.e., greenhouse gases) in the atmosphere cause the greenhouse effect, which creates suitable temperatures for life. The dry atmosphere consists largely of Nitrogen (N_2, 78,08%), Oxygen (O_2, 20,90%) and Argon (Ar, 0,93%) (see figure 1.1). The remaining 0,09% are the so-called trace gases, which profoundly affect the atmosphere's chemistry and the earth's radiative balance. The atmosphere's water content varies greatly depending on the meteorological conditions and can range from almost 0 to up to 5%. The atmosphere is divided into layers that differ in composition and temperature.The layer most familiar to us is the so-called troposphere, which extends from the ground to a height of about 10 - 15 km depending on geographical location and is the layer where essentially all the atmosphere's water vapour and clouds are found (see figure 1.2). It is also the layer in which weather happens.

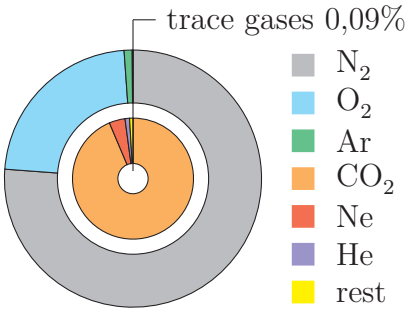

Figure 1.1: The composition of the atmosphere. The remaining trace gases include CH_4, O_3, NO_2, N_2O, NH_3.

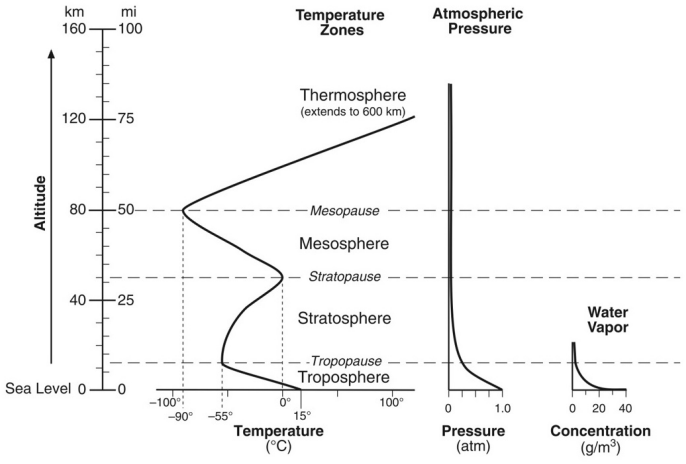

Figure 1.2: The atmosphere's vertical temperature, pressure, and water content profiles [1].

Within the troposphere, the temperature decreases as the altitude increases. This causes warm air masses to rise, resulting in extensive vertical mixing and cloud formation. At the top of the troposphere is the tropopause, i.e. the boundary between the troposphere and the stratosphere. A temperature inversion occurs at this boundary: in the stratosphere, the temperature increases with altitude. Warmer air masses

therefore lie above colder ones, limiting convective mixing. The stratosphere is very dry, and because of its limited mixing and precipitation scavenging, any pollutants that enter it have long life times. Levels of ozone (O_3) peak in the lower part of the stratosphere, at heights of 20-30 km. This region is known as the ozone layer, and its thickness varies spatially and seasonally. O_3 in the stratosphere is formed via the so-called Chapman cycle. UV light of wavelength below 240 nm induces the dissociation of molecular oxygen into atomic oxygen ($O(^3P)$), in accordance with reaction R 1.1 [2]. The $O(^3P)$ then reacts with O_2 in the presence of a third molecule, M, to generate O_3 (see R 1.2).

$$O_2 + h\nu(<240\text{nm}) \longrightarrow O(^3P) + O(^3P) \quad \text{(R 1.1)}$$

$$O_2 + O(^3P) \xrightarrow{M} O_3 + \text{heat} \quad \text{(R 1.2)}$$

$$O_3 + h\nu(<320\text{nm}) \longrightarrow O_2 + O(^1D) + \text{heat} \quad \text{(R 1.3)}$$

$$O_3 + h\nu(400 - 600\text{nm}) \longrightarrow O_2 + O(^3P) + \text{heat} \quad \text{(R 1.4)}$$

The processes responsible for the positive temperature gradient in the stratosphere are the exothermic reactions R 1.2, R 1.3 and R 1.4. O_3 absorbs UV radiation and dissociates into molecular and atomic oxygen with the release of heat, which warms the stratosphere. The excited molecular oxygen $O(^1D)$ is quenched to $O(^3P)$ and can regenerate O_3.

1.2 Air pollution and climate change

The atmosphere's composition is influenced by compounds that are added to it, whose origins may be biogenic (natural) or anthropogenic (due to human activities). Those compounds are typically not inert; they interact with other molecules and particles in the atmosphere and undergo chemical and physical change. Compounds with adverse effects on human health or the global climate are regarded as pollutants. The atmospheric pollutants with the most severe effects on human health are nitrogen oxides (NO_x), tropospheric O_3, and particulate matter; collectively, they are estimated to cause around one hundred thousand premature deaths each year in the European Union [3]. NO_2 levels can reach 200 ppb in polluted atmospheres and peak O_3 levels of 500 ppb have been reported in the most polluted regions [2]. Air pollution also puts ecosystems at risk by causing eutrophication or, in the case of tropospheric O_3, directly damaging

vegetation and reducing crop yields. Climate change and air pollution are intertwined because many air pollutants are also climate forcers. The fifth IPCC report summarized the effects of greenhouse gases and aerosol on the climate [4], as shown in (see figure 1.3).

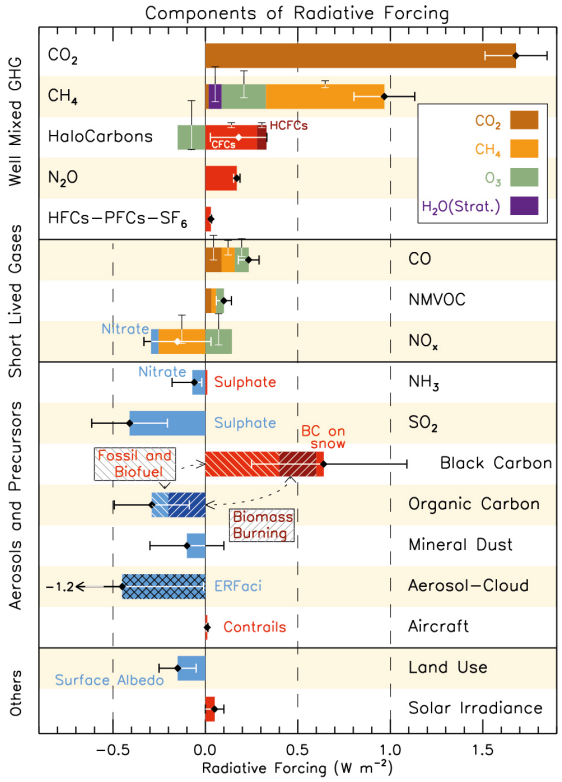

Figure 1.3: Overview of radiative forcing of different greenhouse gases, aerosols and precursors [4].

NO_x is a climate forcer but has become more commonly recognized as an air pollutant in the aftermath of the "diesel-gate" scandal. The term NO_x refers to NO and NO_2, both of which are emitted by combustion engines and play important roles in the oxidation of volatile organic compounds (VOC). VOC oxidation produces alkylperoxy radicals (RO_2) that can react with NO_x to form organonitrates or convert NO into NO_2 (see reactions R 2.4, R 2.5 and R 2.6). NO_2 is photochemically unstable; it undergoes photolysis in visible light (R 1.5) and contributes to tropospheric O_3 formation. O_3 is a substance with both beneficial and harmful effects. Life as we know it depends on stratospheric O_3, which protects earthly life from harmful UV light (R 1.3). However, O_3 is toxic and tropospheric O_3 is a major component of photochemical smog. Stratospheric O_3 is formed by photolysis of O_2 whereas tropospheric O_3 is formed by the photolysis of NO_2 (see R 1.5 and R 1.6). Reaction R 1.7 prevents the simultaneous occurrence of high concentrations of NO and O_3.

$$NO_2 + h\nu(<430nm) \longrightarrow NO + O(^3P) \qquad \text{(R 1.5)}$$

$$O_2 + O(^3P) \xrightarrow{M} O_3 \qquad \text{(R 1.6)}$$

$$O_3 + NO \longrightarrow O_2 + NO_2 \qquad \text{(R 1.7)}$$

Another air pollutant is aerosol, which is defined as a system of particulate matter suspended in air. Depending on their properties, aerosol particles may modify the atmosphere's radiative balance directly by scattering and/or absorbing light, or indirectly

by acting as cloud condensation nuclei (CCN) and thus altering cloud properties [5]. Although atmospheric aerosol particles are considered pollutants and climate forcers, they are also essential for life on earth. Water in the gas phase does not condense readily on its own; its condensation is greatly expedited by the presence of a surface, or nucleus, on which to condense. Aerosol particles provide such surfaces in the atmosphere; in their absence, there would be no clouds and ultimately no rain. A major component of the tropospheric aerosol is secondary organic aerosol (SOA), which has been identified as an important component of smog [5–9]. SOA is formed by the oxidation of VOC in the atmosphere. Because of air quality - climate change interactions, improvements in air quality can affect climate change, and air quality policies designed to reduce the levels of certain pollutants (e.g. SOA) may exacerbate global warming [4].

1.3 Thesis motivation and outline

The aerosols with the strongest effects on air quality and climate are fine aerosols, which consist largely of SOA. The strong effects of SOA on the climate and cloud formation, and its severe negative impact on human health, make it essential to understand the processes and mechanisms that affect its formation and its properties. Low volatility compounds originating from VOC oxidation strongly influence the properties of SOA, new particle formation (NPF), and the condensational growth of fine particles. Organic compounds such as dimer esters [10, 11], carboxylic acids [12–14], and nitrates [15, 16] have been identified to contribute to SOA formation. More recently, highly oxygenated molecules (HOMs) were shown to contribute to NPF [17–21]. Understanding the chemistry and mechanisms that govern the formation of these low volatility compounds is thus paramount. Current models underestimate SOA formation and could be improved by a more comprehensive understanding of the relevant chemical mechanisms. This thesis presents studies on the oxidation of α-pinene, limonene and 1,3,5-trimethylbenzene (TMB), as well as the formation of low volatility compounds during these processes, using state-of-the-art analytical instruments. The general aim of the work was to advance our understanding of VOC oxidation and clarify the reaction mechanisms and oxidation products involved in SOA formation.

More specifically:

- How are dimer esters formed during α-pinene ozonolysis, and how do RH and OH scavengers affect their formation?
- Which nitrates, carboxylic acids, and dimers are formed during limonene oxidation under various conditions?
- How does NO_x influence the oxidation of TMB and particle formation?
- Identify the stoichiometric composition of the gas- and particle-phase products of VOC oxidation. Develop a robust and automated algorithm to extract data from FIGAERO - CIMS thermograms.

The thesis consists of two parts: an extended summary and the appended papers. The extended summary is divided into five chapters. Chapter 1 briefly describes the earth's atmosphere and air pollution, and Chapter 2 provides the reader with a general background on atmospheric chemistry and SOA formation. The instrumentation, lab equipment, and software used in the thesis work are described in Chapter 3, while Chapter 4 summarizes the key findings of the thesis work and answers the research questions presented above. Finally, Chapter 5 presents the conclusions drawn from the results of the laboratory studies and their implications for the atmosphere, and offers some suggestions for future work. The second part of the thesis consists of the appended papers. Paper I presents studies on the formation of low volatility dimer esters during α-pinene oxidation. These esters have been observed in boreal forests and lab experiments; to the author's knowledge, Paper I presents the most comprehensive available list of dimer esters originating from α-pinene oxidation. Papers II and III present studies on the oxidation of limonene; Paper II focuses on organonitrate formation during nitrate-initiated oxidation, while Paper III deals with the formation of carboxylic acids during ozonolysis. Limonene oxidation products were found to be important SOA contributors in both studies. The GUFIT algorithm for analysing thermogram data was developed while analyzing the data presented in Paper III and is developed further in Paper V. Paper IV focuses on anthropogenic rather than biogenic VOC. Specifically, the oxidation of TMB by OH and the effects of NO_x on HOMs and organo nitrate (ON) formation are studied. Potential suppression of NPF is linked to the oxidation product distribution.

2

Aerosol formation and tropospheric chemistry

This chapter begins with an overview of SOA formation. This is followed by a brief introduction to atmospheric chemistry and the oxidation products that contribute to SOA formation.

Contents

2.1 Tropospheric aerosol and SOA formation

Typical lifespans of atmospheric aerosols in the troposphere are between one day and several weeks. Their particles vary greatly in size, but are often divided into four ranges or modes, each of which has different origins and dominant removal processes [22]:

1. Nucleation mode (particle size < ~10 nm)
2. Aitken mode (~10 nm-100 nm)
3. Accumulation mode (100 nm-2.5 µm)
4. Coarse mode (2.5-10 µm)

Modes 1, 2 and 3 are fine particles, while mode 4 consists of coarse particles. The chemical composition of atmospheric aerosol particles is extremely diverse, depends on their source, and varies greatly with location. Whereas aerosol particles belonging to the coarse mode consist mainly of inorganic compounds (mineral dust or sea salt), a large fraction of fine particles consist of secondary organic carbon species, sulfates and ammonia [23]. There is very little mass transfer between fine and coarse particles, and they can be considered chemically distinct.

Unlike directly emitted primary organic aerosol (POA), SOA is formed by low volatility products from VOC oxidation in the atmosphere. SOA precursors include anthropogenic alkanes, alkenes or aromatic hydrocarbons (e.g. TMB) together with biogenic terpenes such as α-pinene or limonene [5]. The contribution of biogenic volatile organic carbon (BVOC) to the global VOC budget is about 90% on average, with isoprene having a contribution of ~50% and monoterpenes ~10%, but these values and the composition can vary temporally and spatially [24]. Hakola *et al.* [25] measured the distribution of monoterpenes emitted by a boreal forest in Hyytiälä, Finland, where α-pinene accounted for 50% of the total monoterpene budget during summer and ~20% in winter. Isoprene and monoterpenes together comprise ~60% of global BVOC emissions and contribute significantly to global SOA formation, even at low yields. Limonene has a pleasant smell and is commonly used in household products. Consequently, it is often found at elevated levels indoors, and contributes to reduced indoor air quality [26, 27]. Because of the dominance and high reactivity of BVOCs, the contribution of anthropogenic volatile organic carbon (AVOC) to SOA formation is primarily important in polluted areas, where SOA contributes significantly to bad air quality.

The limited understanding of SOA-forming processes leads to large uncertainties in SOA budgeting. Bottom up approaches estimate sources between 12-120 Tg a^{-1} and observationally constrained top down estimations range from 120 to 1820 Tg a^{-1} [5, 28]. The near-explicit master chemical mechanism (MCM) calculates the gas phase product distribution resulting from VOC oxidation and can, together with information on thermodynamic properties (e.g. vapor pressures) and partitioning [29], be used to estimate SOA formation in air quality or chemical transport models [30–32]. The quality of the MCM's output depends on the quality of the underlying chemical mechanisms. Models often underestimate SOA levels when compared to real world measurements, suggesting that some mechanisms of organic compound degradation are misrepresented or not properly accounted for, or that some SOA precursors are overlooked [33, 34]. One way to improve the modelling of SOA formation would be to better understand the underlying chemistry. SOA exerts a cooling influence on the Earth and counteracts some of the global mean warming due to greenhouse gases [4]. This potential effect intensifies the need to properly understand SOA formation in the atmosphere.
Put simply, SOA formation occurs via the oxidation of volatile precursor gases into less volatile products that then partition into the particle phase. The initial step in NPF is the formation of molecular clusters from gas phase species which will grow via condensation of vapors with low saturation vapor pressure (VP) and via coagulation [35–37]. The VP is defined as the pressure of a vapor that is in equilibrium with the corresponding liquid, and an organic compound's VP strongly affects its distribution between the gas and particle phases [29]. Unfortunately, there is a lack of reliable VP measurements for the various organic molecules involved in SOA formation [14]. Compounds are classified based on their VP as VOCs or intermediate- (IVOCs), semi- (SVOCs), low- (LVOCs), and extremely low volatile organic compounds (ELVOCs, VP less than $\sim 10^{-7}$ Pa) [17, 38]. Because of the findings reported by Ehn *et al.* [17], HOMs formed from the oxidation of BVOCs have recently attracted considerable research interest [18, 39–42]. A HOM is an organic compound with an O/C ratio of 0.6 or above; most HOMs can be classified as ELVOCs, although recent studies [43, 44] suggest that not all of them satisfy the criteria. ELVOCs are almost entirely found in the particle phase and contribute to NPF [40, 45–48].

The scientific understanding of SOA formation would be greatly improved by a detailed knowledge of the products of VOC oxidation, the mechanisms by which they are formed, and their vapor pressures.

2.2 Atmospheric oxidants

VOCs such as TMB, α-pinene and limonene are SOA precursors. Precursor gases are oxidized in the atmosphere and form products with lower vapor pressures that subsequently partition from the gas phase into the condensed phase. The oxidation processes are initiated by atmospheric oxidants such as radicals (OH, NO_3) or tropospheric O_3, with OH and O_3 being the most important oxidants during daytime. NO_3 is photochemically unstable and is therefore only significant for nocturnal chemistry. OH, NO_3, and O_3 react with organic compounds on very different time scales (table 2.1), and their impact on a VOC's atmospheric fate depends on its structure (see figure 2.1).

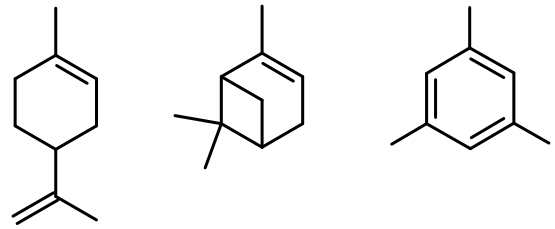

Figure 2.1: Structures of limonene (C_9H_{16}), which has exo- and endocyclic double bonds, α-pinene (C_9H_{16}), which has a single endocyclic double bond, and the aromatic compound TMB (C_9H_{12}).

OH reacts very quickly with most organic compounds, whereas O_3 and NO_3 react much more rapidly with alkenes than with aromatic compounds. Their differing importance in the removal of VOCs is demonstrated by the VOC lifetime calculations shown in table 2.1. OH is a much less selective oxidant than NO_3 or O_3: the lifetime of TMB is approximately 30 minutes in the presence of $2*10^6$ molecules cm^{-3} OH, compared to 427 days or 32 hours in the presence of peak concentrations of O_3 and NO_3, respectively. NO_3 reacts very quickly with alkenes and is important for VOC removal at night. O_3 generally reacts with alkenes more slowly than OH and NO_3, but is a significant oxidant because of its high atmospheric concentration. One source of OH in the lower troposphere is the photolysis of O_3 (see R 1.3) and the subsequent reaction of atomic oxygen with water (R 2.1) [2]. This reaction becomes less important with increasing altitude and decreasing water levels (see figure 1.2).

$$O(^1D) + H_2O \longrightarrow 2\bullet OH \qquad \text{(R 2.1)}$$

Other sources of OH are the photolysis of HONO and H_2O_2, and the reaction of HO_2 with NO when the NO concentration is above 10 ppt. The oxidation of alkenes with O_3 (discussed further in section 2.3) also often gives large yields of OH and can be an important night time source of OH. The OH radical is highly reactive and its

Table 2.1: Estimated lifetimes of TMB, α-pinene and limonene with respect to different oxidants in the atmosphere.

	OH		**O_3**		**NO_3**	
Compound	peak[a]	12 h day time[b]	peak[a]	24 h[b]	peak[a]	12 h night time[b]
TMB[c]	29 min	2.4 hrs	427 d	20.5 yrs	32 hrs	52 d
α-pinene[d]	30 min	2.5 hr	16 min	4.7 hrs	16.5 s	10.8 min
limonene[e]	9.9 min	48 min	6.7 min	1.9 hrs	8.4 s	5.5 min

[a] peak concentrations [molecules cm^{-3}]: 9.84*10^6 OH, 1.23*10^{13} O_3 and 9.84*10^9 NO_3 [2], [b] average concentrations [molecules cm^{-3}]: 2*10^6 OH, 7*10^{11} O_3 and 2.6*10^8 NO_3 [49], [c] k_{TMB+OH} = 5.75*10^{-11}, k_{TMB+O_3} = 2.2*10^{-21}[50], k_{TMB+NO_3} = 8.8*10^{-16}[51], [d] and [e] from [2]: k_{ap+OH} = 5.5*10^{-11}, k_{ap+O_3} = 8.3*10^{-17}, k_{ap+NO_3} = 6.6*10^{-12}, $k_{limo+OH}$ = 1.71*10^{-10}, k_{limo+O_3} = 2*10^{-16} (value for endocyclic double bond), $k_{limo+NO_3}$ = 1.2*10^{-11}. All reaction rates in $cm^3 molecules^{-1} s^{-1}$ and calculated for TMB+OH and all α-pinene with T = 293.15K

concentration is controlled by in situ chemistry rather than transport processes. Typical daytime concentrations range from 2 to 10*10^6 molecules cm^{-3} [2]. The nitrate radical NO_3 is formed by reaction R 2.2.

$$O_3 + NO_2 \longrightarrow O_2 + NO_3\bullet \qquad \text{(R 2.2)}$$

NO_3 dissociates rapidly by absorbing light in the red region of the spectrum to form NO_2 and $O(^3P)$ or NO and O_2. Because this process does not occur in darkness, nighttime concentrations of NO_3 can be as high as several hundred ppt in polluted atmospheres. NO_3 is in equilibrium with NO_2, and forms gaseous dinitrogen pentoxide N_2O_5 as shown in R 2.3.

$$NO_3\bullet + NO_2 \rightleftharpoons N_2O_5 \qquad \text{(R 2.3)}$$

2.3 Ozonolysis

O_3 exhibits specific reactivity towards carbon-carbon double bonds, attacking the π electron system to form a high-energy intermediate known as a primary ozonide (POZ). The POZ decomposes into a carbonyl and a carbonyl oxide via cleavage of the central carbon-carbon bond (I) and one oxygen-oxygen bond (II or III) (scheme 2.1). Each decomposition pathway can form two isomers, with the outer oxygen of the carbonyl oxide pointing to one of the substituting R-groups or the other. The planar carbonyl oxide is known as the Criegee Intermediate (CI). The CI formed from endocyclic compounds such as α-pinene is tethered to the carbonyl group and has the same carbon number as its precursor. However, the carbon number is not preserved when an exocyclic double bond is oxidized. Limonene is a special case in that it has two chemically different double bonds that can be attacked by O_3: one endocyclic and one exocyclic. The attack on the endocyclic double bond proceeds much faster than that on the exocyclic bond ($7*10^{-18}$) [52]. Consequently, the dominant CI derived from limonene will retain the carbon number of the parent compound and the carbonyl group. The term CI* is used to denote a chemically activated CI with a high energy

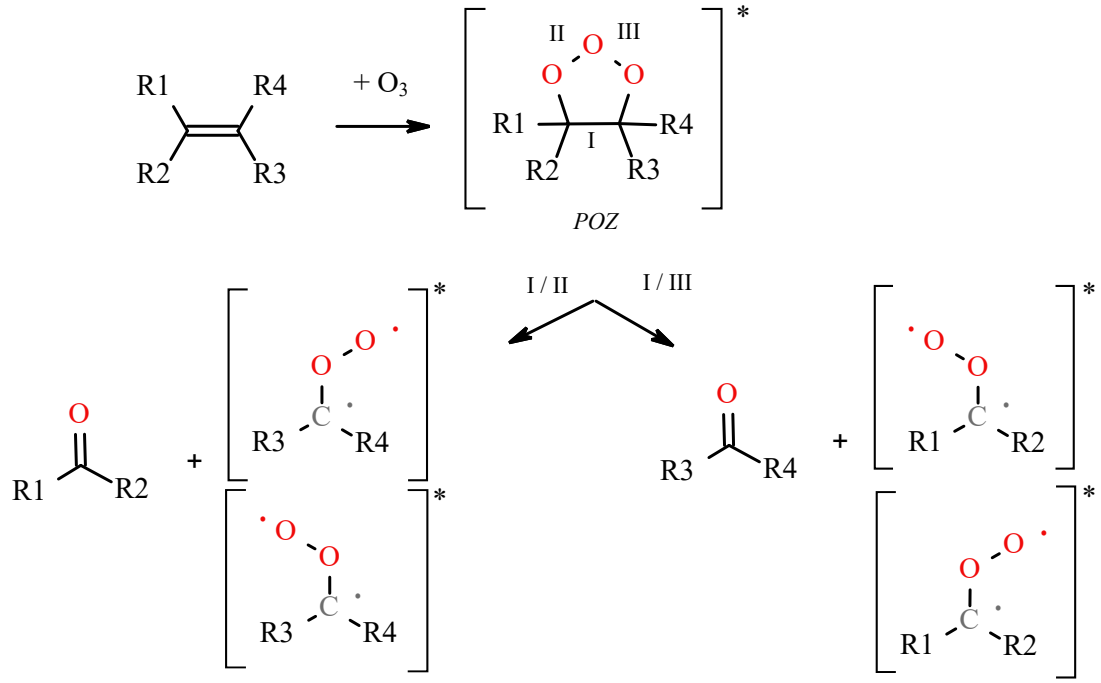

Scheme 2.1: Attack of O_3 on an endocyclic double bond and subsequent formation of POZ and CI*.

content, whereas stabilized Criegee intermediates whose energy content is close to the thermal energy are indicated by the term sCI [53]. Two CI* conformers can be formed, one syn and one anti (figure 2.2). Their reactivities and structures differ; the outer oxygen projects towards a hydrogen in the anti conformer and towards an alkyl group in the syn conformer. There is a high barrier to interconversion of the two conformers, so isomerization is not competitive with the other reactions these CIs can undergo. If O_3 attacks the endocyclic double bond of limonene (R2 and R3 in scheme 2.1 form a cyclic system), the cleavage of bonds I and II can form either a syn- or an anti-CI*. Cleavage of bonds I and III generates only the syn-CI* and yields a carbon radical that is more stable than the one resulting from cleavage at I and II. The reported branching ratios for the two cases are 0.27 (I/II) and 0.73 (I/III), respectively. It is currently believed that the CI* can decompose via a range of reaction channels including the vinyl hydroperoxide (VHP) channel, the ester/hot acid channel, and the oxygen elimination channel, or become collisionally stabilised.

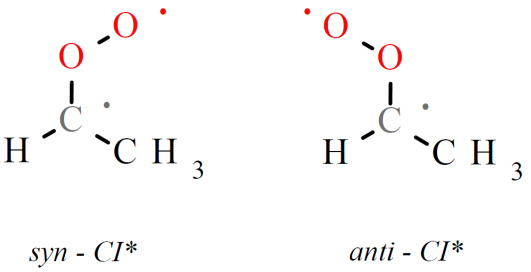

Figure 2.2: Geometry of syn-and anti-CI*.

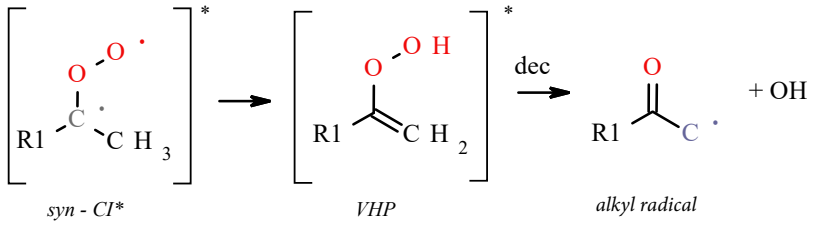

Scheme 2.2: Decomposition of syn-CI* via the VHP channel. Hydrogen in the alkyl radical are omitted.

VHP channel

The OH-producing VHP channel (scheme 2.2) is always more energetically favourable than the ester channel for the syn CI* and is therefore the preferred decomposition pathway [53]. It proceeds via a 1,4 H-shift that forms a hydroperoxide and a carbon-carbon double bond. The resulting VHP is unstable and decomposes via cleavage of the hydroperoxide and double bond. This results in the formation of a carbonyl-bearing alkyl radical and OH. This process is a significant source of atmospheric OH; OH yields of 0.86 for limonene and up to 0.70-0.85 for α-pinene [2, 54] have been reported.

Ester/acid channel

The possible 1,3 H-shift has a high energy barrier [53]. Therefore, instead of forming an acyl radical + OH, anti CI* are more likely to cyclize to form a chemically activated dioxirane (scheme 2.3a). The dioxirane will form a biradical in which one substituent will migrate to form an ester, or, if an α- H is present (in the case of an anti CI*), a carboxylic acid. The formed compound can decompose into a wide variety of products including CO_2, aklyl radicals (R1, R2), OH or acylradicals depending on its structure. Sufficiently large esters or acids may be collisionally stabilised and thus avoid decomposition.

Oxygen elimination channel

CI* can dissociate to a carbonyl compound and O(^{3}P) (scheme 2.3b) but the energy barrier for this pathway is high [53] and branching ratios are generally low. Calvert *et al.* [55] reported the upper limit of O(^{3}P) elimination for α-pinene to be 3% and that for smaller alkenes is even lower.

Collisional stabilisation and subsequent reactions

A sCI may be formed via collisional stabilisation of a CI*. In case of endocyclic alkenes (e.g. limonene and α-pinene) the CI* and carbonyl compound are tethered together and all the energy retained in the molecule is leaving no room for direct sCI formation [53]. Consequently, the yield of sCI formed by collisional stabilisation from endocyclic CI* (15% for α-pinene) is smaller than that from exocyclic CI* (40% from β-pinene). More collisions are needed to stabilize endocyclic CI*, so the stabilization process will be at a competitive disadvantage to unimolecular reactions. The sCI can undergo unimolecular and/or bimolecular reactions with compounds such as H_2O, carbonyls and carboxylic acids. Under atmospheric conditions the reaction with water is believed to be dominant, but recent studies showed that sCI and carboxylic acids can form dimers that were also found in ambient aerosol [56] and suspected to contribute to NPF [57]. If the endocyclic alkene is large enough, the carbonyl oxide can react with the carbonyl group on the other end and form a SOZ. This cyclisation is unfavourable for small sCI and sCI that are hindered by ring strain (α-pinene), but SOZ can still be formed via bimolecular reactions with other carbonyl compounds.

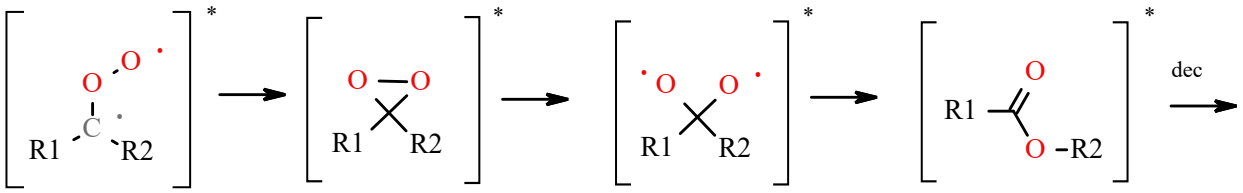

(a) Decomposition via the ester/ hot acid channel.

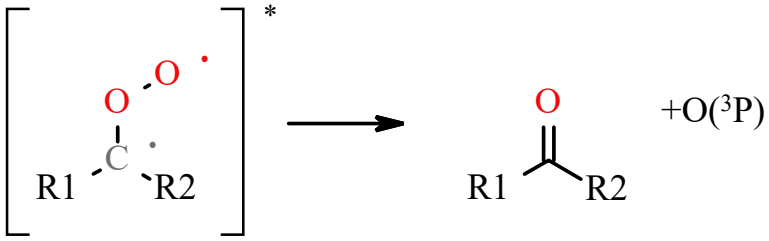

(b) Decomposition via O(^{3}P) elimination and formation of a carbonyl.

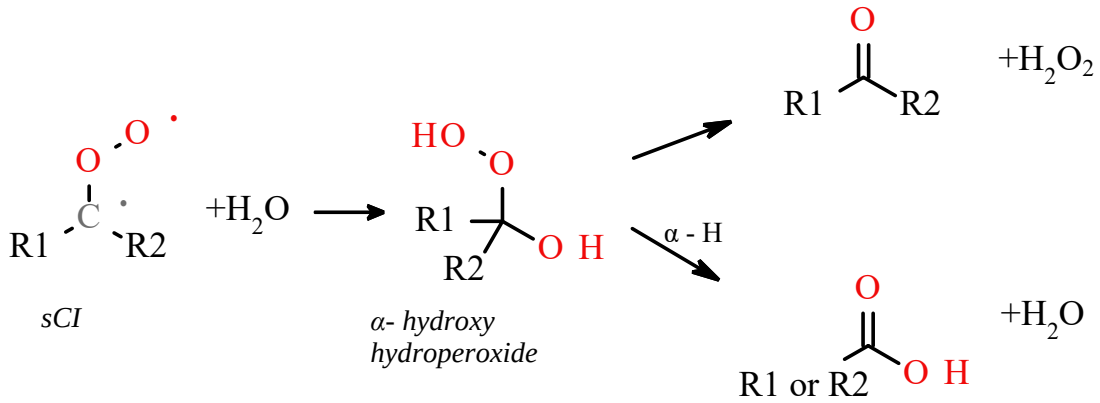

(c) Formation of a carbonyl or carboxylic acid via the reaction of a sCI with water.

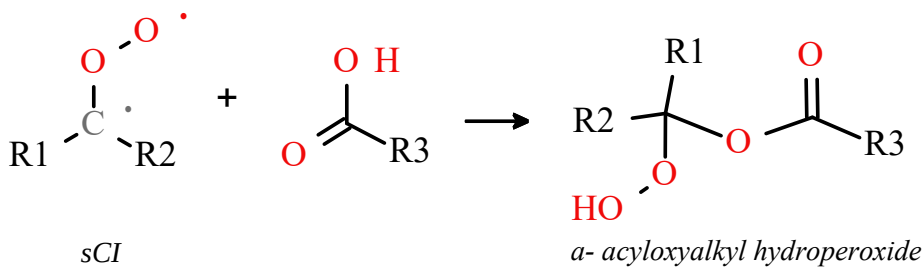

(d) Formation of an α-acyloxyalkyl hydroperoxide dimer through the reaction of sCI with a carboxylic acid.

Scheme 2.3: Different reactions of CI* and sCI.

Water channel

Water is ubiquitous in the atmosphere and will react with sCI. Anti-sCI react more rapidly with water than substituted syn-sCI; the rate coefficients for this process can span 5 orders of magnitude [53]. Given this wide range of reactivity towards water, it is likely that some atmospheric sCI are consumed via other mechanisms. The reaction of sCI with water (scheme 2.3c) proceeds via the formation of an α- hydroxy hydroperoxide with excess energy. This species can be collisionally stabilised or it can decompose, typically forming H_2O_2 and a carbonyl compound. However, if an α-H is present (i.e. R1 or R2 is H), the decomposition process may instead yield a carboxylic acid and H_2O or an aldehyde and H_2O_2.

Reactions with carbonyls and carboxylic acids

Carbonyl compounds react with sCI and form SOZ that can decompose relatively easily unlike compounds formed by the reaction of sCI and carboxylic acids (scheme 2.3d). The reaction of sCI with carboxylic acids leads to formation of thermally stable high molecular weight compounds with an α-acyloxyalkyl-hydro peroxide group [53, 56–59]. Those dimers have low enough vapour pressures to potentially contribute to new particle formation, unlike the products of the sCI + carbonyl pathway. Paper I presents extensive studies on the formation of acyloxyalkyl-hydro peroxide bridged dimers from α-pinene and O_3.

2.4 OH and NO_3 initiated chemistry

The mechanism of oxidation by OH and NO_3 differ from those of ozonolysis because no POZ is produced. The initial reaction step in both cases is either H abstraction or electrophilic addition (see scheme 2.4). OH is a less selective oxidant than NO_3 or O_3 (see table 2.1) and it is often called the detergent of the atmosphere. OH can react by addition to a double bond or aromatic system or by H abstraction, depending on temperature. At room temperature and below, electrophilic addition dominates. The reaction of NO_3 with aromatics is usually too slow to be of atmospheric importance, but it reacts rapidly with alkenes. H abstraction from a carbon preferentially occurs at the site that yields the most substituted and thus most stable radical. Radical stability is directly related to the strength of the corresponding C-H bond, and tertiary C-H bonds (bond strength: 96 kcal mol^{-1}) are weaker than secondary (98 kcal mol^{-1}) and primary (101 kcal mol^{-1}) C-H bonds [2]. The reactions of aldehydes, alcohols and carboxylic acids with OH are faster than with NO_3 and proceed via H abstraction. The alcohol O-H bond (104 kcal mol^{-1}) is stronger than the alkyl C-H bond (96 kcal mol^{-1}), so alkyl hydrogen atoms are abstracted preferentially. Aldehydic H are usually weakly bonded (87 kcal mol^{-1}) and are abstracted in

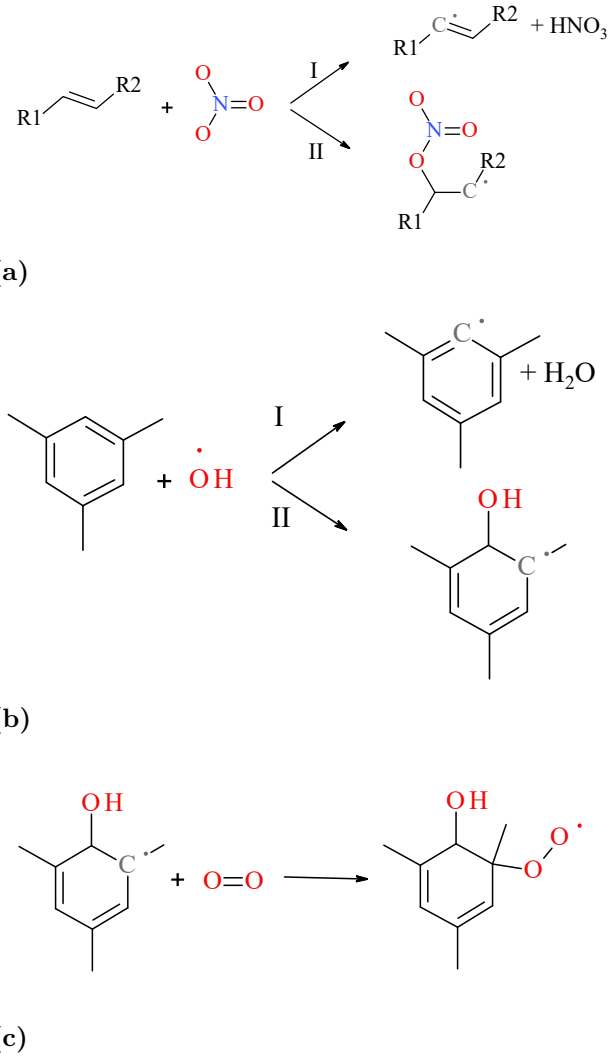

Scheme 2.4: Initial attack of NO_3 and OH on unsaturated (2.4a) or aromatic (2.4b) systems (TMB) via H abstraction (I) or electrophilic addition (II). The produced alkyl radicals react rapidly with O_2 to form an alkylperoxy radical (2.4c).

preference to alkyl hydrogens. Carboxylic acids form H-bonded complexes with OH, leading to abstraction of the carboxylic H and the formation of RO and H_2O. In ketones, OH and NO_3 abstract a H from the alkyl chain. In general, radical attack will produce an alkyl radical (except in the case of carboxylic acids + OH) that rapidly reacts with O_2 to form an alkylperoxy radical, RO_2 (scheme 2.4).

2.5 RO_2 and RO chemistry

The lifetime and fate of RO_2 radicals depends strongly on their environment, as shown in the general overview (figure 2.3) of VOC degradation. At high NO_x concentrations, RO2 reacts rapidly with NO to form an alkoxy radical and NO_2 (reaction R 2.4). However, larger RO_2 radicals may isomerize and form stable alkyl nitrates (reaction R 2.5). Acylperoxy radicals may react with NO_2 to form so called PAN-like compounds, which are semi-stable and can be transported downstream of heavily polluted areas (reaction R 2.6). There they can decompose into RO_2 and NO_2 again, thus introducing pollutants to suburban or rural areas [60]. RO_2 radicals can also react with HO_2 or other RO_2 radicals to form a wide range of products (reactions R 2.7-R 2.12). In bimolecular reactions with HO_2, path R 2.7 is believed to be dominant. Under anthropogenically influenced conditions, the reaction RO_2 + NO will dominate over RO_2 + HO_2, but in remote regions where HO_2 and NO concentrations are roughly equal, (4-8 ppt), the removal of RO_2 by HO_2 can compete.

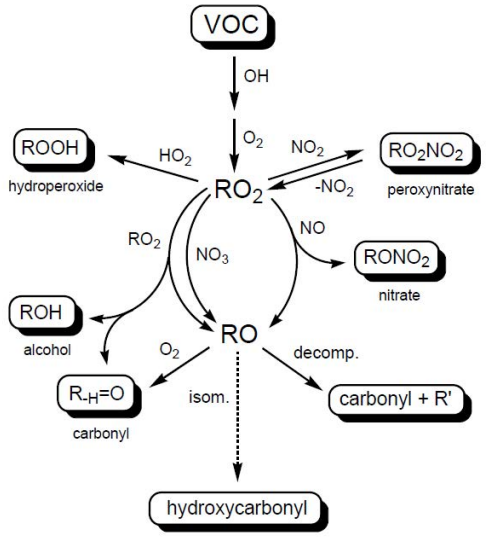

Figure 2.3: General mechanism of OH initiated oxidation of VOC, from Hallquist *et al.* [5].

$$RO_2\bullet + NO \longrightarrow (ROONO)^* \longrightarrow RO\bullet + NO_2 \qquad (R\,2.4)$$

$$\longrightarrow (RONO_2)^* \longrightarrow RONO_2 \qquad (R\,2.5)$$

$$R(O)O_2\bullet + NO_2 \xrightarrow{M} R(O)O_2NO_2 \qquad (R\,2.6)$$

$$RO_2\bullet + HO_2\bullet \longrightarrow ROOH + O_2 \quad (R\,2.7)$$

$$\longrightarrow \text{carbonyl} + HO_2\bullet + O_2 \quad (R\,2.8)$$

$$\longrightarrow ROH + O_3 \quad (R\,2.9)$$

Te reactions of bimolecular RO_2 species are expected to proceed via the formation of an excited intermediate (ROOOOR)* that decomposes into RO (via R 2.10), an alcohol and carbonyl (via R 2.11), or a covalently bound peroxy-bridged dimer (via R 2.12)

$$RO_2\bullet + RO_2\bullet \longrightarrow (ROOOOR)^* \longrightarrow 2RO\bullet + O_2 \quad (R\,2.10)$$

$$\longrightarrow ROH + RCHO + O_2 \quad (R\,2.11)$$

$$\longrightarrow ROOR + O_2 \quad (R\,2.12)$$

The RO radical may undergo intramolecular H abstraction (R 2.13), reaction with O_2 and subsequent formation of HO_2 (R 2.14) or decomposition via β-bond scission (R 2.15). Reaction R 2.14 requires the presence of an α-H. Intramolecular H abstraction is more important for larger molecules and is unfavourable for compounds with fewer than 4 carbon atoms. β-bond scission (R 2.15) produces a carbonyl compound and an alkyl radical, which will react further. The reactions of RO with NO (R 2.16) and NO_2 (R 2.17) can also be important at sufficiently high concentrations.

$$RH{-}{-}RO\bullet \longrightarrow \bullet R{-}{-}ROH \quad (R\,2.13)$$

$$RHO\bullet + O_2 \longrightarrow R(O) + HO_2\bullet \quad (R\,2.14)$$

$$R{-}RO\bullet \xrightarrow{\beta-scission} R\bullet + R(O) \quad (R\,2.15)$$

$$RO\bullet + NO \longrightarrow RONO \quad (R\,2.16)$$

$$RO\bullet + NO_2 \longrightarrow RONO_2 \quad (R\,2.17)$$

2.6 HOMs formation

The intramolecular isomerization or auto oxidation of RO_2 via H shifts (R 2.18) is known to occur during the oxidation of organic compounds, high temperature combustion, and food spoiling, but was thought to be irrelevant in atmospheric oxidation because of large barrier heights [61]. The presence of functional groups in RO_2 is now known to lower this barrier height, and auto oxidation was recently proposed to be important for HOMs formation in atmospheric systems [39]:

$$\mathrm{HR{-}{-}RO_2\bullet} \xrightarrow{H-shift} \mathrm{\bullet R{-}{-}ROOH} \xrightarrow{+O_2} \mathrm{RO_2\bullet{-}{-}ROOH} \longrightarrow \longrightarrow \quad \text{(R 2.18)}$$

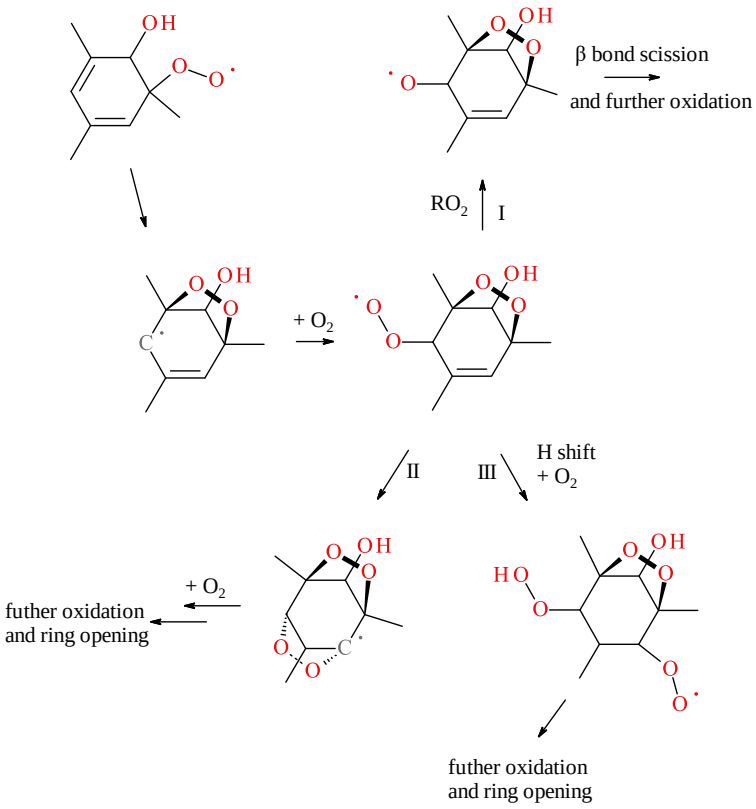

Scheme 2.5: HOMs formation from TMB via auto oxidation and formation of multiple ring systems. Radical chain continuation from scheme 2.4c.

This unimolecular reaction was found to be responsible for the formation of low volatility oxidation products in forested regions with low NO_x emissions [18, 39]. RO_2 molecules may survive up to 100 s before finding a suitable reaction partner under such conditions, leaving enough time to for auto oxidation. Auto oxidation products are termed HOMs, based on their multi functionality and and O/C ratios above 0.6. They are also known as ELVOCs, because of their low vapour pressures. The two terms are often used interchangeably but recent studies [43, 44] suggest that not all HOMs are ELVOCs. In the first step of HOMs formation, an RO_2 radical is formed by the attack of an oxidant on

a VOC and the resulting alkyl peroxy radical abstracts an H from another C, creating a hydroperoxide functionality and a new radical center, to which O_2 adds. This forms a new alkyl peroxy radical, which continues the chain. This cascade reaction (R 2.18) can be repeated several times, introducing several oxygen centers into the molecule before being terminated by a uni- or bimolecular reaction. Mentel *et al.* [41] describe possible termination reactions and the associated mass spectrometric patterns. The reaction of RO_2 (m/z = x) with HO_2 (reaction R 2.7) can lead to the formation of a hydroperoxide (m/z = x + 1), while reactions of one RO_2 radical with another can lead to the formation of a carbonyl (m/z = x - 17) and a hydroxy compound (m/z = x – 15) via reaction R 2.11 or dimer formation (m/z = 2x – 32, with O_2 as the leaving group in reaction R 2.12). The reaction between RO_2 and NO or another RO_2 can result in the formation of RO (m/z = x - 16). In the latter case, an internal H shift may lead to the formation of a hydroxyl and subsequently an alkyl peroxy group, which can participate in further autooxidation sequences. The sequences will be shifted by 16 in the latter case, and the resulting termination products may overlap. Aromatic compounds may give rise to bicyclic or multicyclic peroxy radicals. Scheme 2.5 shows potential HOMs formation pathways from TMB. Pathway I is the postulated fate of bicyclic peroxy compounds after reaction with RO_2 [2], and pathway II is that suggested by Molteni *et al.* [62], which introduces a second oxygen bridge. Pathway III, postulated by Wang *et al.* [63] for isopropylbenzene, proceeds via a H-shift and subsequent addition of O_2 to the resulting alkyl radical. The formation of different HOMs generations based on the numbers of OH attacks was described in a recent publication by Molteni *et al.* [62]. The oxidation of TMB (C_9H_{12}) resulted in HOMs with 12, 14, and 16 H. Compounds with 12 H were classified as first generation HOMs formed by the reaction of OH with TMB. Compounds with 16 H originated from the reaction of OH with first generation HOMs, while compounds with 14 H could have originated from either first or second generation radicals, depending on the termination reaction. The recombination of RO_2 may lead to dimer formation. When this happens, the number of H in the dimer will depend on the generation of the recombining RO_2: it will be 26 H if two first-generation RO_2 recombine, 28 H for the recombination of a first and second generation species, and 30 H for the dimerisation of two second generation RO_2.

3

Materials and methods

State-of-the-art scientific instrumentation was used to study and understand the complexity of atmospheric oxidation. This chapter introduces the experimental tools and instruments used in this thesis.

Contents

3.1 G-FROST

The Gothenburg Flow Reactor for Oxidation Studies at low Temperatures (G-FROST) is a laminar flow reactor mounted vertically in a temperature-controlled housing and is used to study oxidation processes (typically with O_3 and NO_3 as the oxidants) in the dark. It was used in Paper I, Paper II and Paper III. The reactor is a 191 cm long pyrex glass cylinder that is coated with halocarbon wax and has a diameter of 10 cm. Oxidants and VOCs are added to the cylinder via separate lines. The humidity in the system is controlled by bubbling zero air (Linde Gas, Model N-GC6000) through a temperature-controlled gas wash bottle filled with Milli-Q water in the exhaust flow. VOCs are added by passing N_2 over a characterized capillary diffusion cell and their concentration is adjusted by changing the temperature of the aforementioned source. The total inflow into G-frost is 1.6 lpm and the outflow through a funnel-shaped sample outlet is 0.96 lpm. Only the central part of the flow is taken for further analysis to reduce wall effects on the formed aerosol, resulting in a median residence time of 240 s. O_3 is produced outside G-FROST by photolysing pure O_2 using UV light (UVP Pen-Ray® Mercury Lamps $h\nu$ = 185 nm) according to reactions R 1.1 and R 1.2. O_3 concentrations are adjusted by changing the exposure of O_2 gas to the UV lamps. The ozonolysis of alkenes can result in large OH yields (see scheme 2.2). To study pure ozonolysis without OH-induced secondary chemistry, OH scavengers are used. 2-butanol is a commonly used OH scavenger that

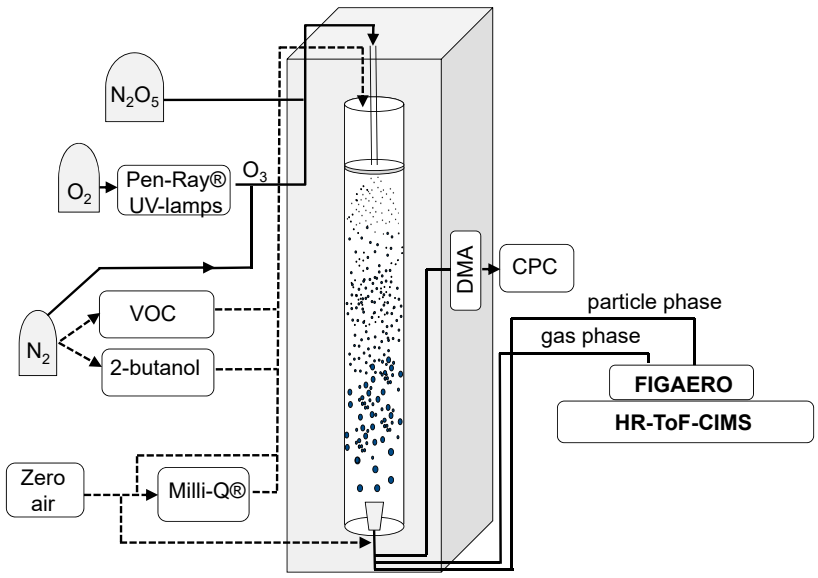

Figure 3.1: Schematics of G-FROST connected to the FIGAERO - ToF - CIMS and SMPS where either O_3 or NO_3 (from N_2O_5, see R 2.3) can be used as oxidant. Adapted from Paper II and Paper III.

reacts with OH to form methacrolein and HO_2 with a yield of 64% [64] and thus alters the radical population by increasing the HO_2/RO_2 [65]. To produce NO_3 radicals, solid N_2O_5 synthesised by reacting O_3 with pure NO_2 and passing the flow through a cold trap (- 78.5 °C) is placed in a diffusion vial and held at constant temperature (-23°C).

3.2 Go:PAM

The Gothenburg Potential Aerosol Mass chamber (Go:PAM) is a quartz flow reactor with a length of 100 cm and a diameter of 9.6 cm. The original PAM was introduced by Kang *et al.* [66]; it was improved and further developed into Go:PAM by Watne *et al.* [67]. The sample flow is added to the center of the flow tube and the oxidant flow containing O_3 and H_2O is introduced through a perforated disk to ensure even distribution of oxidants over the tube's cross-section. O_3 is produced outside of Go:PAM using the same method as for G-FROST. Only the central part of the laminar flow is collected (via a funnel) for further analysis to reduce wall effects. Go:PAM can generate OH radicals for oxidation studies via O_3 photolysis in the presence of water vapour (R 1.3 followed by R 2.1). Photolysis is induced by two 10 W Phillips UV lamps ($h\nu$ = 254 nm) mounted outside the glass cylinder. The rate of OH radical production is varied by changing the O_3 and H_2O concentrations and measured indirectly based on the decay of SO_2 [66]. Go:PAM was used in Paper I and Paper IV.

3.3 FIGAERO - ToF - CIMS

The FIGAERO - ToF - CIMS consists of two separate units, the Filter Inlet for GAses and AEROsols (FIGAERO) and the Time of Flight Chemical Ionization Mass Spectrometer (ToF - CIMS), both developed by Aerodyne. A wide range of ions can be used for chemical ionization; in this thesis acetate (CH_3COO^-), iodide (I^-) and nitrate (NO_3^-) ions were used.

3.3.1 ToF - CIMS

A mass spectrometer can only detect ionized species. Several methods exist to convert neutral molecules into ions, one of which is chemical ionization. The advantage of chemical ionization is that it is a relatively soft method that causes minimal fragmentation of the targeted molecule and so preserves molecular information. Another advantage of chemical ionization is that the ionizing agent can be selected to target specific functional groups. Acetate ions in declustering mode are used to specifically ionize acids [68], minimizing sensitivity to non-acidic compounds. Iodide selectively ionizes oxygenated or nitrogen-containing compounds [69] by H-bonding and clustering with alcohols, acids, and aldehydes. Acetate is thus more selective than iodide and provides additional information on functionalization. To generate acetate reagent ions, a flow of 0.02 lpm acetic anhydride in ultra-high purity (UHP) N_2 ($C_4H_6O_3$ Sigma Aldrich, puriss p.a. $\geq$ 99%, kept in a gas wash bottle at 20°C) was merged with 2.2 lpm UHP N_2 before passing through the ionizer. Iodide ions were generated by passing UHP N_2 over a lab-built permeation tube kept at room temperature and filled with CH_3I (Alfa Aesar, 99%) before passing through the ionizer. In both cases, the ionizer was a commercially available ^{210}Po source (NDR, P-2021, α-emitter) and electrons are generated according to reaction (R 3.1):

$$N_2 \xrightarrow{He^{2+}} {N_2}^+ + e^- \qquad \text{(R 3.1)}$$

The reagent was then ionized by dissociative electron attachment (R 3.2 and R 3.3).

$$CH_3I + e^- \longrightarrow I^- + CH_3\bullet \qquad \text{(R 3.2)}$$

$$C_4H_6O_3 + e^- \longrightarrow CH_3COO^- + CH_3CO\bullet \qquad \text{(R 3.3)}$$

Highly oxidized compounds (O/C > 0.6) can be detected as adducts by means of ${NO_3}^-$ chemical ionization atmospheric pressure inlet time of fight (CI - API - TOF) mass spectrometry [18, 41, 70]. Instead of the Ion Molecule Reaction Chamber (IMR) used in acetate and iodide ionization mode, the "wall less" Eisele inlet [71] was used to measure low volatility compounds. Unlike the IMR, which has turbulent mixing, the nitrate inlet is a coaxial laminar flow tube with a sheath flow consisting of clean air and HNO_3 vapor that is ionized near the inlet of the flow tube (R 3.4).

$$(HNO_3)_n + e^- \longrightarrow (HNO_3)_{n-1} \cdot {NO_3}^- \qquad \text{(R 3.4)}$$

The source of α-particles in the nitrate inlet is ^{241}Am and the release of electrons happens according to R 3.1. The sample is added to the middle part of the sheath flow and wall contact is minimized. Sample molecules form negative clusters with NO_3^- (R 3.5) and a negative voltage applied to the walls helps prevent wall losses. Strong acids such as H_2SO_4 may be deprotonated in the process(see R 3.6).

$$(HNO_3)_{n-1} \cdot NO_3^- + MH \longrightarrow (HNO_3)_{n-1} + NO_3^- \cdot MH \quad \text{(R 3.5)}$$

$$(HNO_3)_{n-1} \cdot NO_3^- + MH \longrightarrow (HNO_3)_{n-1} + HNO_3 + M^- \quad \text{(R 3.6)}$$

The nitrate inlet is subsampled with a critical orifice and the ion clusters are preserved on their way to the ToF region. Compounds ionized by iodide or nitrate will be detected as clusters whereas acetate-ionized compounds will be declustered and the carboxylic acid group deprotonated. These different treatments require a tunable environment, which the ToF - CIMS provides. The ToF - CIMS consists of five differentially pumped chambers, and is depicted schematically in figure 3.2.

In the IMR, iodide or acetate ions react with the sample gas, whose admission is regulated via a critical orifice (1.9 lpm) and which flows orthogonally to the reagent gas from the ionizer (admitted at 2 lpm via a critical orifice supplied by O'Keefe Controls Co.). The IMR is kept at a pressure of 90 mbar during acetate ionization (R 3.7) and 200 mbar during iodide ionization (R 3.9), by throttling the Varian SH-112 Dry Scroll Vacuum Pump accordingly. The reagent ions react with the sample molecules for a duration of 0.1 s before being sub-sampled via another critical orifice into the Collisional Dissociation Chamber (CDC). When using nitrate ionization, the Eisele inlet, operating at atmospheric pressure, is mounted to the CDC instead of the IMR. The CDC contains a Small Segmented RF-only Quadrupole (SSQ) and is kept at 2 mbar by pumping with a TriScroll 600 Series Dry Scroll Vacuum Pump. The 6 segments of the SSQ enable the creation of an electric field to dissociate or preserve weakly bound molecular clusters, depending on the electrical field strength. To preserve clusters during iodide ionization, a weak electric field is applied in the SSQ. Conversely, during acetate ionization, a strong electric field is applied to destroy clusters (R 3.8). In the latter case, dissociation probably occurs between the exit of the CDC and the entrance aperture of the next Big Segmented Quadrupole (BSQ) [72].

$$CH_3COO^- + MH \longrightarrow CH_3COO^- \cdot MH \quad \text{(R 3.7)}$$

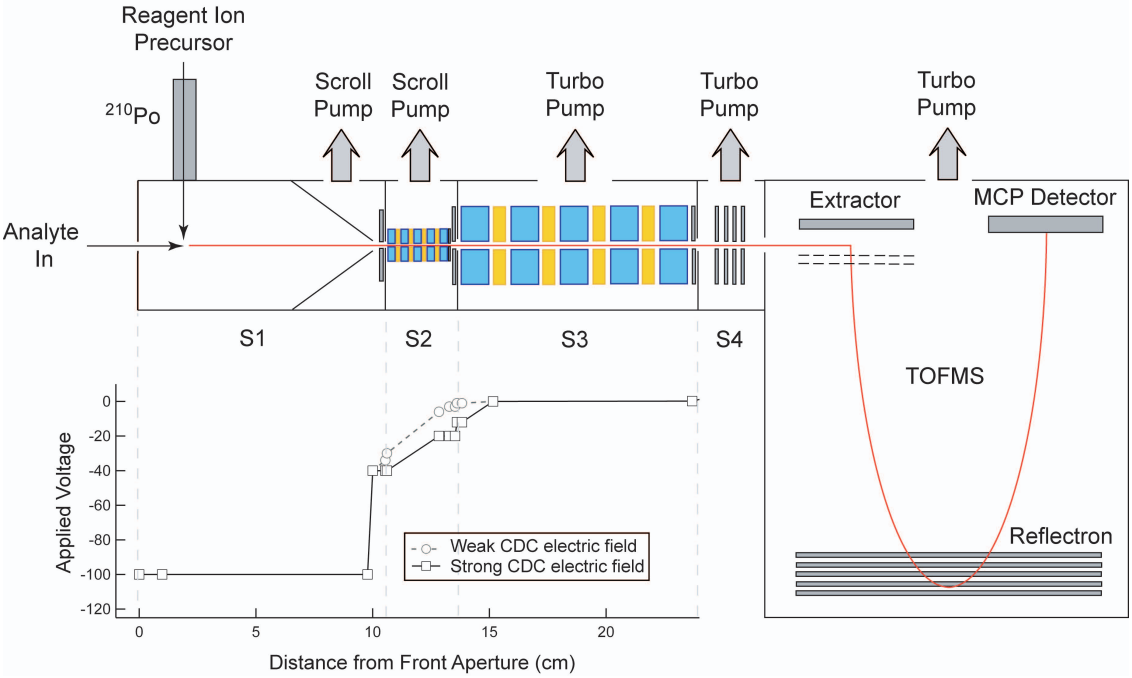

Figure 3.2: Schematic depiction of the HR - Tof - CIMS [72] used with varying ionisation methods in Paper II, Paper III and Paper IV.

$$CH_3COO^- \cdot MH \longrightarrow CH_3COOH + M^- \quad \text{(R 3.8)}$$

$$I^- \cdot (H_2O)_n + M \longrightarrow n(H_2O) + MI^- \quad \text{(R 3.9)}$$

The BSQ, ion lenses and the ToF region are pumped by a Pfeiffer Split-Flow 310 turbo pump and pressures decrease from approximately $1*10^{-5}$ mbar in the BSQ to $1*10^{-6}$ mbar in the orthogonal ToF extractor. The BSQ and ion lenses focus the ion beam further to match the requirements of the ToF. Ions are accelerated by a DC pulse and the time from extraction to hitting the multi- channel plate is in on the order of 1 - 50 µs.. The ToF t is related to the mass m and charge z of an ion by equation 3.1.

$$t = k * \sqrt{\frac{m}{z}} \quad (3.1)$$

with the constant k being determined by mass calibration (measuring the ToF of ions with known m/z). This extraction happens very rapidly ($50kHz$) and data for successive extractions are averaged and saved at a typical rate of $1Hz$.

3.3.2 FIGAERO

The ToF - CIMS can only measure molecules in the gas phase, so to analyse the chemical composition of the particulate phase, all condensed phase molecules must be brought into the gas phase. The FIGAERO inlet, which is described in detail by Lopez-Hilfiker *et al.* [73], is a multi-port add on for the Tof - CIMS system and is mounted on the inlet part of the IMR. FIGAERO enables the analysis of gas phase chemical composition while simultaneously collecting particles on a 25mm 1µm PTFE (Zefluor™) filter. After collecting particles on the filter, it is automatically moved by an actuator arm to the desorption position and the gas phase sampling port is blocked. The collected particles are desorbed with heated N_2 and their chemical composition is analysed. The whole system is automated, and the collection and desorption times as well as the temperature profile are programmable.

3.3.3 CIMS data analysis

Data obtained from the ToF - CIMS were analysed using the data analysis package "Tofware" (www.tofwerk.com/tofware) written in the Igor Pro (Wavemetrics, OR, USA) environment. Before analysis, the raw data were pre-averaged to 0.0167 Hz (1 min) with the Tofware pre-averaging function to optimise processing time. Instrument functions such as the mass spectral baseline, integration regions for unit mass stick data, and peak shapes and peak widths as functions of m/z were determined. Generally, only reagent ion peaks and mass calibrants were used to derive empirically determined peak shapes to avoid double peaks. These user-defined peak shapes were used for mass calibration, and the calibrants were chosen to cover a wide range of m/z. Perfluorinated heptanoic acid (PFHA) was added as mass calibrant because of its high molecular weight and ability to be detected by all three ionisation schemes. One or more peaks were fitted to the mass calibrated spectrum at each m/z, and chemical formulas were assigned to each peak. Isotope patterns were calculated relative to the fitted amplitude of the parent peak and constrained in the HR peak fitting. To construct a thermogram from FIGAERO data, the signal intensity from the HR fitting of a compound assigned a specific m/z was plotted against the desorption temperature. The peak area and temperature of maximum signal intensity (T_{Max}) were obtained using the GUFIT algorithm.

4

Results and discussions

Chapter 4 answers the research questions posed in section 1.3. The key findings on dimer, nitrate and carboxylic acid formation from α-pinene, limonene as well as TMB oxidation are covered. Paper I - Paper III focus on the oxidation products and mechanisms of α-pinene and limonene, while Paper IV deals with the influence of NO_x on the oxidation of TMB. Paper V discusses the GUFIT algorithm developed for data analysis in Paper III and shows how it can be used for vapor pressure estimations. This chapter summarizes the results of four published peer-reviewed papers (Papers I - III and V) and one manuscript in preparation (IV).

Contents

4.1 Dimer formation

Paper I-Paper III and Paper IV present studies on the formation of dimers from α-pinene, limonene and TMB . The experiments reported in all four papers were done using the G-FROST or Go:PAM facility in Göteborg, and oxidation products in the gas and particle phases were detected with different mass spectrometric methods.
As reported in Paper I, 28 different dimeric esters were detected in the particle phases of SOA samples generated by oxidizing α-pinene with O_3 in the laboratory. All of them exhibited similar fragmentation patterns in the UHPLC/MS analysis, suggesting that they were formed from similar monomeric units. Conversely, dimer formation was largely suppressed when α-pinene was oxidized with OH in the PAM chamber. Dimers comprised 5-16% of the mass of SOA formed by ozonolysis but were absent from the gas phase, presumably because of their low vapour pressures. Of the 28 dimers found in the laboratory experiments, 15 were previously detected in ambient aerosol samples collected in Hyytiälä, Finland. The absence of dimers in the OH-initiated experiments indicates that O_3 is crucial in their formation, and Paper I suggests that they are formed via the gas phase reaction of sCI with carboxylic acids. The theory of gas phase production of dimer esters is supported by recent ambient measurements reported by Mohr *et al.* [19] and a laboratory study by Zhang *et al.* [74]. Dimers may also form via the self-coupling of RO_2 radicals (see reaction R 2.12), which will become increasingly significant as the concentration of precursors increases [75]; this process should not be limited to O_3-initiated oxidation. However, Paper I shows that the concentrations of the 8 most abundant dimers increased with the levels of HO_2/RO_2, suggesting that they were primarily formed via reactions involving sCI and carboxylic acids rather than RO_2 self-coupling. The levels of the other 20 dimers fell in the presence of OH scavengers, suggesting that although O_3 is essential for the initial oxidation step in dimer formation, OH promotes the formation of certain esters, probably by influencing carboxylic acid formation. Experiments under humid conditions showed that dimer formation increased with humidity, which is not entirely consistent with the assumed predominance of the sCI + water reaction. However, no general dependence on humidity was observed for carboxylic acids. The concentrations of dimer esters derived from α-pinene in the ambient Hyytiälä samples was relatively high (~1% of total PM_1), and their low volatility paired with their rapid gas phase formation indicates that they may be important contributors to NPF and particle growth in the atmosphere. While Paper I focused on dimers derived from α-pinene, many

other VOCs can undergo dimerization processes similar to those that were observed. Paper II describes the formation of dimers during NO_3-initiated oxidation of limonene. These dimers resided almost entirely in the particle phase and accounted for 37 ± 7% of the particle phase signal on average. Dimer species having more than 10 carbons were found in the m/z range of 580-700 (clustered with iodide) and can be regarded as ELVOCs. Consequently, they are likely to play key roles in SOA formation and NPF [18, 19]. The two dominant dimer families (which had 10 members between them) were the dinitrate dimers $C_{19}H_{28}N_2O_x$ with x = 10-15 and $C_{20}H_{29}NO_y$ with y = 14-17. These species have T_{max} desorption temperatures of 100 - ~160 °C and their thermograms feature double peaks, which were attributed to thermal decomposition fragments from even higher order oligomers. The O/C ratios of the dimers observed in this work were lower than those of the corresponding monomers. Unlike in Paper I, where dimerization was attributed to the reaction of sCI and carboxylic acids, the dimerization observed here was presumed to involve the loss of NO_x or HNO_3, which could explain the dimers'comparatively low O/C ratios. The results presented in Paper II cannot support any firm mechanistic conclusions, but because the experiments were performed under dry conditions, direct hydrolysis of monomers was unlikely. With the thermodynamically stable HNO_3 as a leaving group, the reaction would produce dimers with lower O/C ratios than the parent monomers, in accordance with reactions R 4.1 and R 4.2.

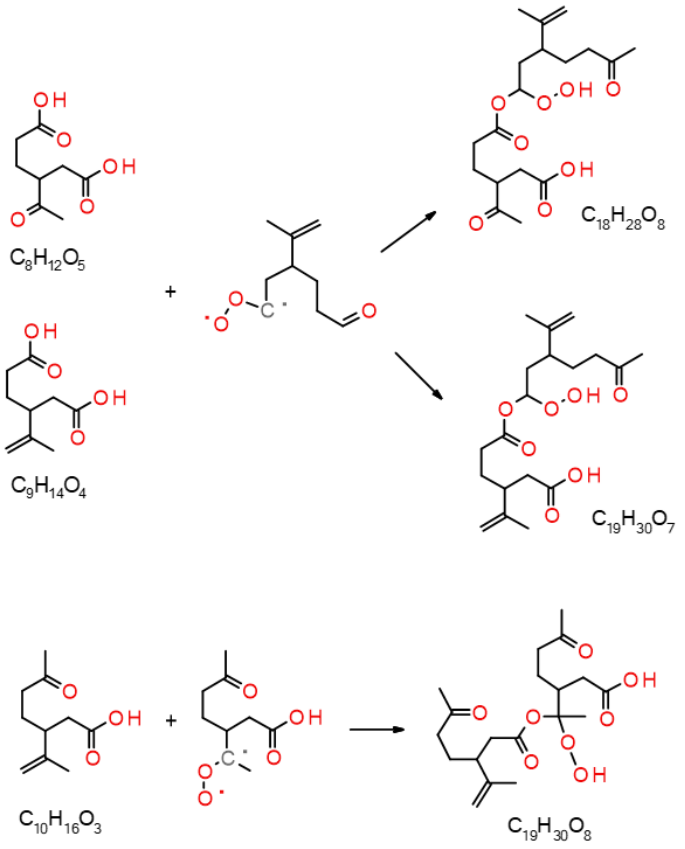

Scheme 4.1: Dimerisation mechanisms involving carboxylic acids and a sCI formed from limonene (upper) and limononic acid (lower) oxidation

$$C_{10}H_{15}NO_6 + C_{10}H_{15}NO_8 \longrightarrow C_{20}H_{29}NO_{11} + HNO_3 \quad \text{(R 4.1)}$$

$$C_{10}H_{16}N_2O_9 + C_9H_{13}NO_8 \longrightarrow C_{19}H_{28}N_2O_{14} + HNO_3 \quad \text{(R 4.2)}$$

Owing to the loss of HNO_3 in the dimerisation process, the fragments resulting from thermal decomposition of the dimers will differ from those of the precursors involved in their formation, and attributing monomer fragments to specific dimers is difficult.

Unlike the dimer formation processes studied in Paper II (up to 40% contribution of dimer to particle phase signal), the limonene ozonolysis experiments described in Paper III did not yield large amounts of detectable dimers (see figure 4.1). The FIGAERO ToF-CIMS was used in both studies, but with different chemical ionisation schemes. In the experiments described in Paper III, acetate was used as the reagent ion to specifically target carboxylic acids. Dimerisation was suggested to occur by the formation of α-acyloxyalkyl hydroperoxides in the gas phase from sCI and carboxylic acids followed by partitioning into the particle phase; the resulting dimers should not be detected under acetate ionization if their sole carboxylic group was lost in the dimerisation process. Scheme 4.1 shows the possible formation of $C_{18}H_{28}O_8$ and $C_{19}H_{30}O_7$ by the reactions of ketolimonic acid and limonic acid, respectively, with an endocyclic limonene sCI, as well as the reaction of limononic acid and the limononic sCI to form $C_{19}H_{30}O_8$. All three dimers retain carboxylic acid groups, making them detectable under acetate ionization.

HOMs dimer formation has been reported in previous studies and found to be important for NPF [18, 41, 62]. Their formation in the gas phase was attributed to the RO_2 self reaction (R 2.7). Oxidation of TMB with OH radicals yielded 18C dimers with the general formula $C_{18}H_{26-30}O_{10-16}$ that generated ions in the mass range 460-560 m/z (figure 4.4), as reported in II. The contribution of gas phase dimers to the overall signal increased with the level of OH exposure, and the presence of NO_x generally reduced dimer formation. For example, the dimer contribution in experiment NO_x3_L (which had a similar OH exposure to experiment 1 but a 3.5-fold higher $NO_x/\triangle$ TMB ratio) was 57% lower than that in experiment 1. In experiment NO_x9, which had a still lower OH exposure and a higher $NO_x/\triangle$ TMB ratio, the dimer contribution was reduced by a further 37%. Conversely, the monomer contribution in experiments NO_x3_L and NO_x9 were only 19% and 23% lower, respectively, than that in experiment 1. This effect was less pronounced in experiments with high OH exposure. The contribution of

dimers to the total signal was highest in experiment 3 and slightly lower in experiment 4 even though the latter had a higher OH exposure. Particle formation was observed in experiment 4, so it is likely that some of the dimers (which have low volatility and a high particle formation potential) were lost to the condensed phase. The contributions of the dimers $C_{18}H_{26}O_{10}$ and $C_{18}H_{28}O_{11}$ in experiment 1 were 4.4% and 4.0%, respectively, and these compounds generated the highest peaks in experiments 2 and 3 (figure 4.4a). The oxidative generation of an oxidation product is determined by its H content, as described in section 2.6. Dimer populations with 26, 28, and 30 H were observed; those with 28 H predominated at higher OH exposures. R 4.3 implies that the rate of dimer formation should increase with the square of the HOMs-RO_2 concentration, so their relative abundance should increase with the RO_2 concentration. High OH exposures lead to rapid TMB consumption and high RO_2 concentrations in general.

$$\mathrm{HOMs{-}RO_2\bullet + HOMs{-}RO_2\bullet \longrightarrow HOMS{-}dimer + O_2} \qquad \text{(R 4.3)}$$

This increased oxidation potential at higher OH exposures will also increase levels of second generation RO_2 ($C_9H_{15}O_x$) and thus the production of dimers with the formula $C_{18}H_{28\text{-}30}O_x$. The second generation dimers with 30 H were generally less abundant than other dimers, and made the greatest contributions in experiments 3 and 4.

4.2 Organo nitrate formation from limonene and TMB

Oxidation by the nitrate radical is important in nocturnal atmospheric chemistry, and recent lab and ambient studies [76, 77] have emphasized the importance of organo nitrates(ON) from monoterpenes for nocturnal SOA formation and as NO_x reservoirs. Paper II describes the nitrate-induced oxidation of limonene under dry conditions. Several nitrated species (monomers and oligomers, differentiated strictly based on their numbers of carbons) were observed and shown to contribute substantially to the gas and condensed phase (89.5 ± 1.4%) signals. Compounds included in the MCM accounted for only 43.5 ± 3.2% of the experimentally observed total monomer signal. All the observed non-MCM species contained nitrogen and were highly oxidized (with over 6 O atoms) or oligomeric. The strongest signals were attributed to species with 8-10 carbons (see table 4.1). The dominant monomer family was $C_{10}H_{15}NO_x$ (where $5 < x < 9$), with $C_{10}H_{15}NO_6$ being the dominant species in the gas and particle phases in most

Table 4.1: Averaged contribution over all experiments for each family to the SOA signal with T_{max} ranges and number of species observed in each family. The number of monomers that desorb at high temperatures are noted in parentheses. From Paper II.

Class	No.	Family	No. observed in family	Average contribution	T_{max} range (°C)
Monomers	m1	$C_{10}H_{15}NO_x$	5 (1)	23.0 ± 8.0 %	74–152
	m2	$C_{10}H_{18}N_2O_x$	2 (0)	8.8 ± 2.4 %	66–70
	m3	$C_{10}H_{16}N_2O_x$	5 (1)	6.7 ± 2.2 %	52–154
	m4	$C_{10}H_{17}NO_x$	5 (2)	5.3 ± 2.7 %	59–159
	m5	$C_8H_{11}NO_x$	3 (0)	4.7 ± 1.4 %	68–81
	m6	$C_9H_{13}NO_x$	4 (0)	3.0 ± 1.1 %	70–75
	m7	$C_9H_{15}NO_x$	4 (0)	2.0 ± 0.7 %	64–76
Dimers	d1	$C_{20}H_{29}NO_x$	4	7.1 ± 3.3 %	100–154
	d2	$C_{19}H_{28}N_2O_x$	6	5.0 ± 2.2 %	101–157
	d3	$C_{20}H_{27}NO_x$	4	2.8 ± 1.2 %	101–151
	d4	$C_{20}H_{24}N_2O_x$	3	2.0 ± 1.7 %	125–157

experiments. Dinitrate formation results from secondary chemistry, which may be more relevant for the doubly unsaturated limonene than for other monoterpenes. Some of the acquired thermograms featured double peaks, which were attributed to thermal fragmentation of oligomers at higher temperatures. Double peaks were most common for monomeric species but also occurred for some dimers. For each compound, the first temperature maximum value was taken to be the true T_{max}. A clustering analysis was performed using the measured T_{max}, MW and carbon numbers as inputs. The best clustering and separation of ions was achieved when a model based on five clusters was adopted. Clusters 1 and 2 primarily contained C7-C9 and C9-C10 monomers, respectively, with cluster 1 having slightly lower T_{max} values. Cluster 0 consisted of thermal fragments with 7-10 carbons that desorbed at T < 120°C. 87% of cluster 1 and 69% of cluster 2 compounds had thermograms with double peaks and were therefore also assigned to cluster 0. Clusters 3 and 4 contained more and less volatile dimers, respectively. As the N_2O_5/limonene ratio increased, the fraction of detected dimers decreased but the fraction of monomer signal desorbing at high temperatures increased. This suggests that the absolute rate of dimer formation may be independent of the N_2O_5/limonene ratio but the proportion of thermally unstable dimers rises as the ratio increases.

ON formation during OH-induced TMB oxidation at high NO_x/VOC levels was reported in Paper IV. These ON species were among the most abundant oxidation products in all NO_x experiments other than NO_x1_H, in which particle formation occurred and which used a higher OH exposure than any other experiment with added NO_x (see table 4.2 and figure 4.3). The general stoichiometric formulae for the observed ON compounds were $C_9H_{12\text{-}18}NO_{6\text{-}13}$ and $C_9H_{12\text{-}18}N_2O_{8\text{-}15}$ (figure 4.4). The compounds generating the strongest signal in experiment NO_x1_H (which used an $NO_x/\triangle$ TMB of ~1) were $C_9H_{15}NO_{10}$ (6.1.%), followed by non-nitrated HOMs. In experiment NO_x3_H $NO_x/\triangle$ TMB ~3) the dominant oxidation product was the ON $C_9H_{15}NO_{10}$ (10.4% contribution). Conversely, in experiment NO_x3_L (which used a similar $NO_x/\triangle$ TMB but a lower OH exposure), the dinitrate $C_9H_{14}N_2O_{10}$ was the dominant product (10% contribution). The contributions of first generation nitrates and dinitrates generally increased with the $NO_x/\triangle$ TMB, as shown in table 4.2, and were highest in experiment NO_x9 $NO_x/\triangle$ TMB ~9), where ON accounted for 70% of the total signal. This general increase in ON levels was accompanied by a decline in particle formation. The reduced levels of gas phase HOMs dimers and the absence of particles as possible condensation sinks for those dimers suggests that NO may scavenge RO2 according to reaction R 2.5) and form ON at the expense of dimers.

4.3 Carboxylic acids from limonene oxidation

Carboxylic acids may be very important in SOA formation because of their low vapour pressures. Therefore, Paper III investigated the influence of radical chemistry, water, and the oxidant concentration on their formation from limonene. A total of 33 experimental conditions were examined, and the general effect of the studied parameters on SOA formation were consistent with our previous findings (for example, SOA formation was observed to increase with humidity) [78]. The number of different carboxylic acids identified in the gas and particle phases greatly exceeded the numbers reported in earlier limonene oxidation studies [79–84]. The most important acids in the gas and particle phases, averaged over all experiments, were $C_7H_{10}O_{3\text{-}4}$, $C_8H_{12}O_{4\text{-}5}$, $C_9H_{14}O_{4\text{-}5}$ and $C_{10}H_{16}O_{3\text{-}4}$. The product distribution in all experiments was also calculated with the MCM (v 3.3.1) to compare the measured carboxylic acid product distribution to the expected one. The calculations suggested that the concentrations of most of the acids should be strongly OH-dependent, and should be higher in the absence of

2-butanol. Indeed, several MCM species were predicted to have near-zero concentrations in the presence of 2-butanol. This was not consistent with the experimental results. Additionally, the only acid whose concentration was predicted to be only weakly dependent on humidity was $C_{10}H_{16}O_3$. To assess the complexity of the gas and particle phases, the summed contributions of the 10 most abundant acids to the total acid signal were investigated. The particle phase was found to have a more complex composition than the gas phase: the 10 strongest ion signals accounted for 56-91% of the total signal in the gas phase and 47-92% of that for the particle phase. Figure 4.1 shows a typical particle phase mass spectrum. Signals of monomeric acids (i.e. acids with 10 or fewer carbons) are observed between 130 and 250 *m/z*. Dimers with >10 carbons generated signals above 300 *m/z* but were much less abundant (relative to monomeric acids) than in other studies (see Paper I, Paper II and Paper IV) and their formation is discussed in more detail in section 4.1. The experimental results show that the acid signals were generally stronger under humid conditions. The positive correlation between humidity and the signals of acids such as $C_{10}H_{16}O_3$, $C_9H_{14}O_3$ and $C_8H_{14}O_3$ was especially clear in the presence of an OH scavenger, when oxidation proceeded exclusively via ozonolysis. The strength of the particle phase acid signals correlated positively with humidity, which is consistent with the findings of Jonsson *et al.* [78] who attributed increases in the SOA number and mass to the formation of more low-volatile species under humid conditions. Under low and medium O_3 conditions, the acid signals were stronger when mixed oxidation was permitted. At the highest O_3 concentrations, the acid signals were weaker when no 2-butanol was used to scavenge OH. Levels of RO_2, HO_2 and OH correlated more strongly with the $C_{10}H_{16}O_3$ and $C_9H_{14}O_3$ signals under dry conditions, highlighting the importance of radical chemistry when the water pathways for CI breakdown are inaccessible. The higher the O_3 concentration, the more likely it is that the second double bond will be oxidised. The strength of the $C_7H_{10}O_{2\text{-}3}$ signals correlated negatively with the O_3 concentration in the presence of 2-butanol, suggesting that these acids are unsaturated. $C_{10}H_{16}O_3$ (limononic acid) and $C_8H_{14}O_3$ (MCM compound C823OH), correlate positively with O_3, which is surprising for unsaturated compounds; it may be that these species are formed more rapidly than they are destroyed by ozonolysis. The negative correlation between the O_3 concentration and the strength of the acid signals is stronger under dry conditions and for acids with fewer carbons. Under humid conditions, the O_3 concentration correlates positively with signal strength for most acids. These complex correlation patterns were not reproduced at all by the MCM. A comparison of the calculation and of the experimental results shows that in contrast to the predictions, many acids can be formed in the absence of OH.

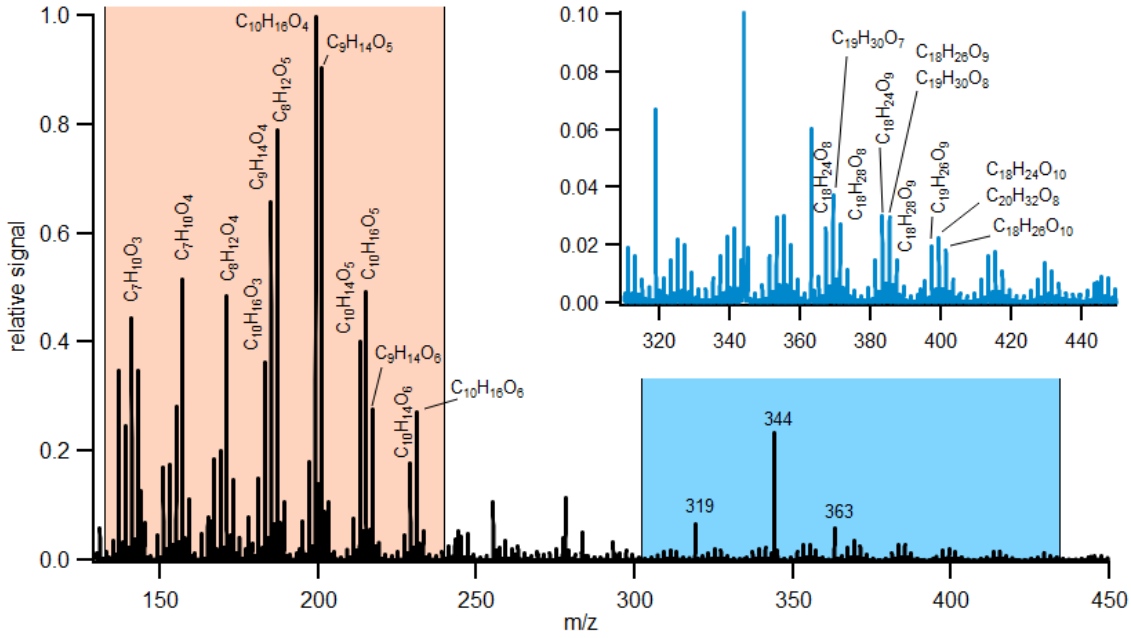

Figure 4.1: Representative mass spectrum of carboxylic acids in the particle phase formed from limonene ozonolysis (1000 ppb O_3 and 150 ppb limonene in the presence of 2-butanol). The orange region shows the monomer products and the blue region dimer compounds. The peaks at 319, 344 and 363 *m/z* are associated with the mass calibrant PFHA. From Paper III.

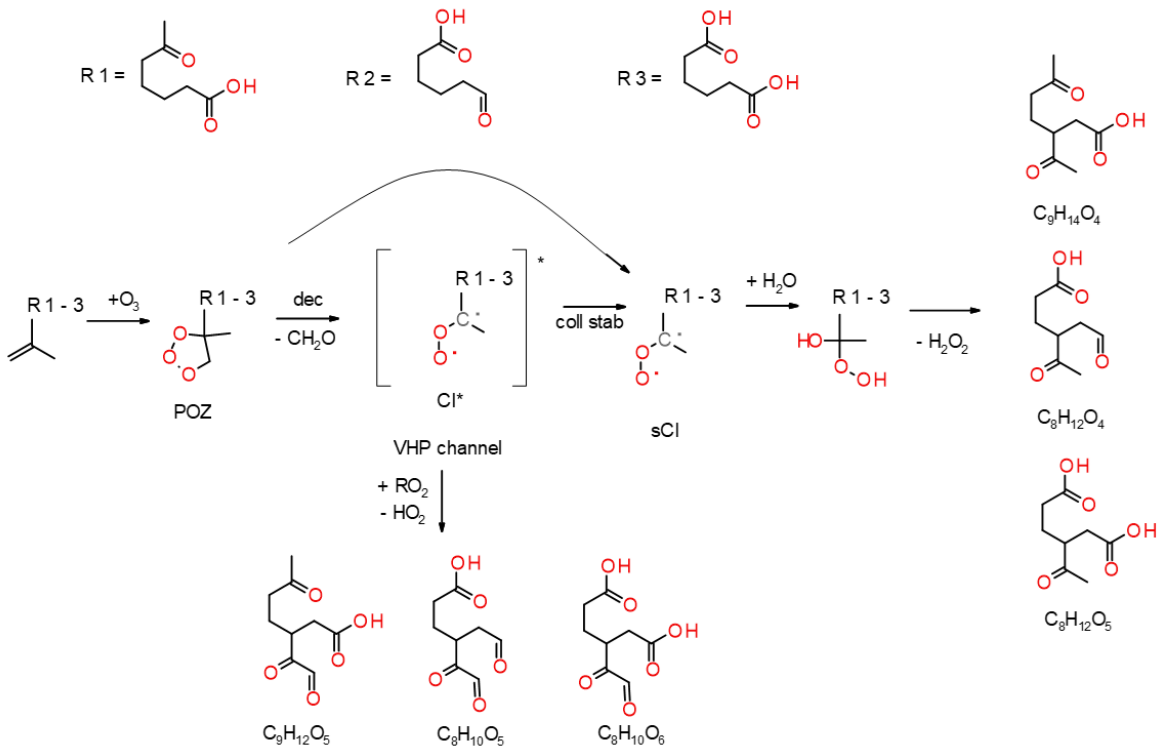

Scheme 4.2: Proposed reaction mechanisms for the unsaturated acids $C_{10}H_{16}O_3$ (limononic, R1), $C_9H_{14}O_4$ (limonic, R2) and $C_9H_{14}O_4$ (limonalic, R3) with O_3. Possible oxidation products are $C_8H_{10}O_{5\text{-}6}$, $C_8H_{12}O_{4\text{-}5}$, $C_9H_{12}O_5$ and $C_9H_{14}O_4$. From Paper III.

For example, the current mechanism suggests that the levels of the C7 acids $C_7H_{10}O_{4\text{-}5}$

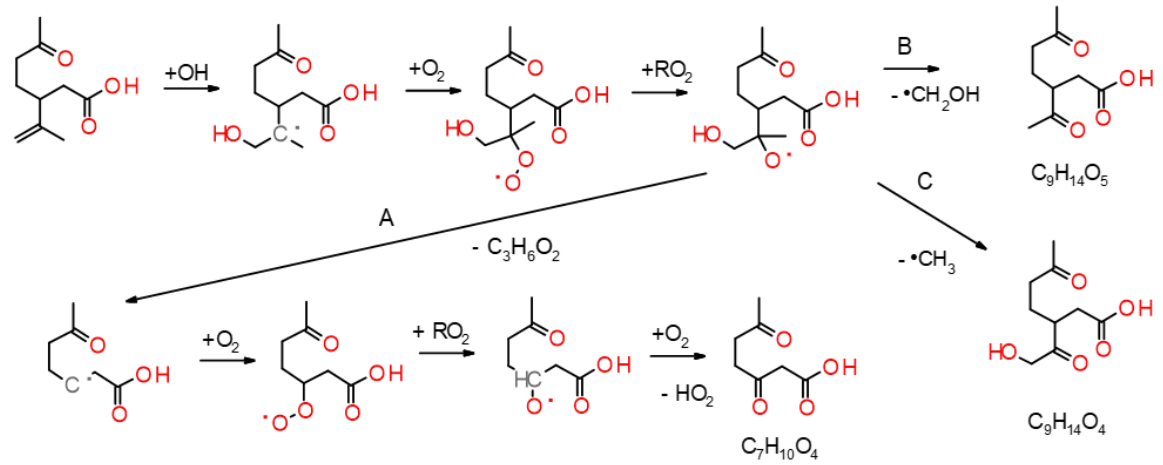

(a) Additional source of $C_9H_{14}O_{4\text{-}5}$ and $C_7H_{10}O_4$.

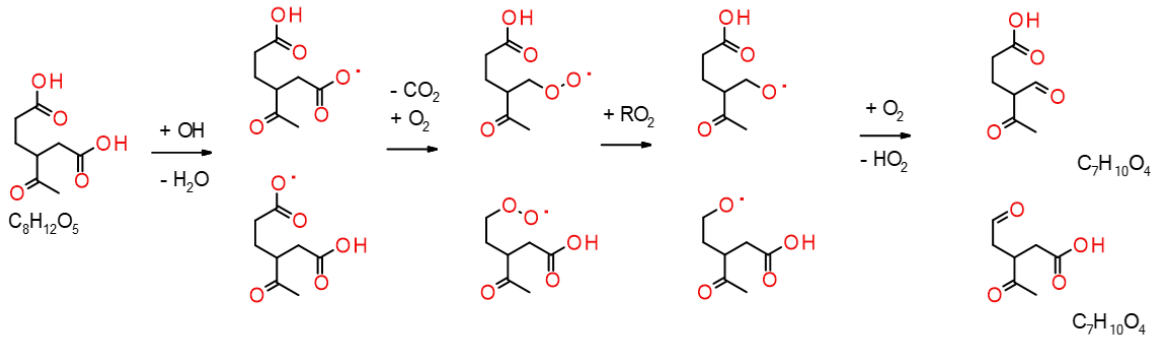

(b) Fomation of $C_7H_{10}O_4$.

Scheme 4.3: Proposed reaction mechanisms of OH with limononic acid (4.3a) and ketolimononic acid (4.3b), from Paper III.

and $C_7H_{12}O_3$ should be near 0 in the presence of 2-butanol, but both compounds were formed in large quantities in experiments including the scavenger. Moreover, the signals of many acids correlated quite strongly with humidity, whereas the model suggests that only $C_{10}H_{16}O_3$ should exhibit such a correlation. This discrepancy between the model and experimental results suggests that there are mechanisms involving OH and water that are not taken into account in the current limonene mechanism. Scheme 4.2 shows the proposed mechanisms for the reactions of limononic, limonic, and limonalic acid with O_3. In all three cases, the remaining double bond is attacked and a C9 CI* is formed by splitting off formaldehyde. The reaction pathways that are open to the CI* will provide additional sources of C8 and C9 acids such as

$C_9H_{12}O_5$, which (to our knowledge) has not previously been described in the literature. The remaining double bond can also be oxidised by OH as shown in scheme 4.3a. Only unsaturated acid products can react with O_3. Oxidation by OH is a possible sink for saturated compounds; in the case of $C_8H_{12}O_5$ (scheme 4.3b), this may lead to the formation of $C_7H_{10}O_4$. Figure 4.2 A shows the contributions of the 10 most abundant compounds in the gas and particle phases averaged over all experiments. Results for the experimental conditions most closely resembling atmospheric conditions (low concentrations of O_3 and limonene concentrations, high humidity, and no 2-butanol) are shown in figure 4.2 B. The reaction mechanisms proposed in Paper III qualitatively explain 65% of the gas phase and 50% of the particle phase composition, on average. For the atmospheric case, 74% of the gas phase and 42% of the particle phase signals are explained qualitatively by the reaction mechanisms proposed in Paper III.

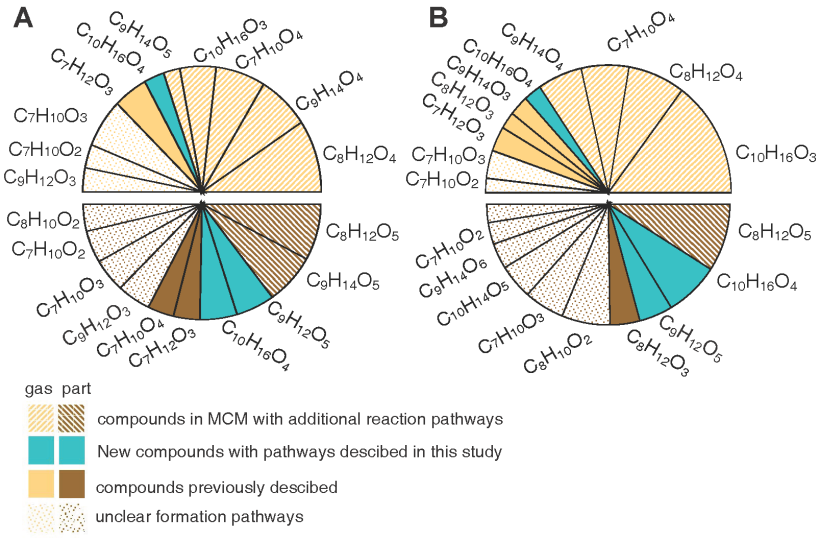

Figure 4.2: Contributions of the 10 most abundant acids averaged over all experiments (A) and for experiment 1, which best represents the atmospheric case (B). The top and bottom halves of the wheels show gas and particle phase data, respectively.

Table 4.2: Reaction conditions and particle production in different experiments. $NO_x/\triangle$ TMB ranged from 0.1 to ~9. $\triangle$ TMB (*ppb*) and OH exposure ($*10^{10}$ s*molecules*cm^{-3}) were explicitly calculated in Facsimile. Particle number density is reported in $\#cm^{-3}$. The contributions of different HOMs and nitrate generations are reported as percentages of the total oxidation product signal.

	1	**2**	**3**	4	$\mathbf{NO_x9}$	$\mathbf{NO_x3}_L$	$\mathbf{NO_x3}_H$	$\mathbf{NO_x1}_H$
$NO_x/\triangle$ TMB	0.93	0.51	0.1	0.11	9.11	3.52	3.2	1.17
OH exposure	0.35	0.71	3.77	21.1	0.63	0.79	3.06	9.1
$\triangle$ TMB	5.4	9.9	26.3	30	9	10.9	24.6	29.8
particles	-	-	60 ± 14	1610 ± 217	-	-	-	170 ± 50
$\mathbf{C_9H_{12}O_x}$	11.3	7.8	3.5	5.4	8.5	9.3	5.9	5.4
$\mathbf{C_9H_{13}O_x}$	5.7	4.5	3.3	2.1	6.0	7.0	5.6.	4.2
$\mathbf{C_9H_{14}O_x}$	8.3	10.8	9.9	17.4	4.3	6.6	8.0	13.0
$\mathbf{C_9H_{15}O_x}$	5.6	7.2	9.3	4.1	2.4	3.3	4.6	4.7
$\mathbf{C_9H_{16}O_x}$	4.8	8.0	7.7	14.5	1.5	2.5	4.8	10.3
$\mathbf{C_{18}H_{26}O_x}$	8.5	9.1	8.5	9.2	0.8	2.0	2.7	6.0
$\mathbf{C_{18}H_{28}O_x}$	7.1	9.9	9.3	11.0	0.4	1.2	2.6	6.9
$\mathbf{C_{18}H_{30}O_x}$	0.7	1.0	2.3	2.6	0.4	0.4	0.9	1.7
$\mathbf{C_9H_{13}NO_x}$	6.2	4.7	0.6	0.6	26.8	17.1	10.1	4.8
$\mathbf{C_9H_{15}NO_x}$	6.4	5.6	0.7	0.9	3.7	10.3	14.5	8.5
$\mathbf{C_9H_{14}N_2O_x}$	2.1	1.7	0.9	1.1	18.7	11.8	7.5	1.9

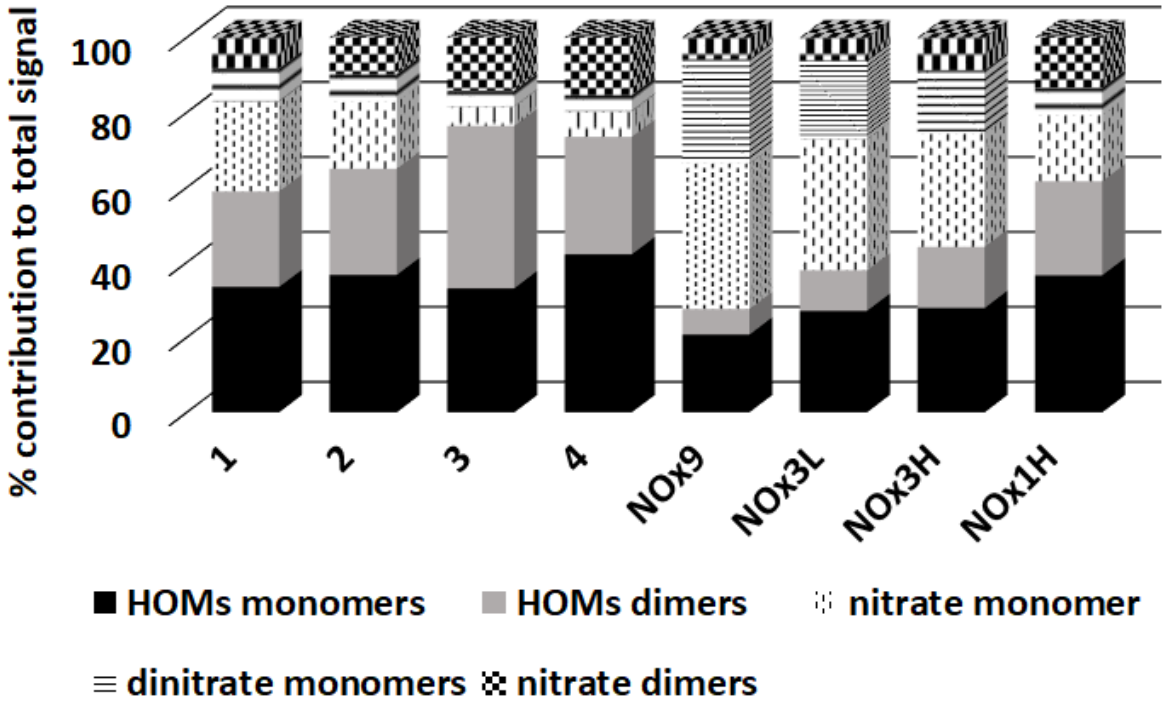

Figure 4.3: Relative contributions of different compound classes to the total signal.

4.4 Effect of NO_x on HOMs and particle formation

The products of OH-initiated TMB oxidation in NO_x-free environments have been identified as HOMs and are linked to potential NPF in urban environments [62, 63]. HOMs formation relies on RO_2 radical propagation reactions, but RO_2 can be scavenged by NO and transformed into ONs or RO. Paper IV examined the effects of NO_x on HOMs formation and particle formation potential by studying TMB oxidation at NO_x/VOC ratios commonly observed in polluted urban environments [85]. A kinetic box model based on the MCM [86] and extended with HOMs formation reactions [18, 87, 88] was used to simulate the chemistry under these conditions in Go:PAM. The formation of HOMs monomers and dimers as well as ON with one or two N was observed, producing ions in the mass 270-560 *m/z* as shown in figure 4.4. The observed +16 *m/z* pattern in the mass spectra (which stems from RO isomerization and subsequent RO_2 formation) and the observed H patterns are consistent with previous studies on HOMs formation and termination reactions [41, 89, 90]. The monomers detected in this study had the general formula $C_9H_{12\text{-}16}O_{6\text{-}11}$. HOMs compounds were the dominant products in all experiments without added NO_x. The contributions of first generation HOMs monomers ($C_9H_{12}O_x$) and first generation open shell species ($C_9H_{13}O_x$) decreased with increasing OH exposure, while the opposite was true for the contributions of $C_9H_{14}O_x$, second generation HOMs ($C_9H_{16}O_x$), and $C_9H_{15}O_x$ radicals because of the greater likelihood of a second OH oxidation step. The bulk contribution observed in experiment 4 was similar to that in a recent study on HOMs formation from TMB by Molteni *et al.* [62], but those authors observed higher contributions of $C_9H_{14}O_x$ and $C_{18}H_{26}O_x$ compounds. Substantial particle formation ($1610 \pm 217\ cm^{-3}$) was observed in experiment 4, which used the highest OH exposure. However, elevated NO_x levels suppressed particle formation. Given the observed increase in ON levels and the simultaneous decrease in dimer levels and particle formation in experiments with added NO_x, we propose that the general reaction HOMs-RO_2 + NO competes with HOMs-RO_2 self-reaction, and that the reduction in dimers is responsible for the reduced particle formation potential. More specifically, we suggest that first and second generation nitrates, and dinitrates, are formed by reactions R 4.4 - R 4.8. First generation (HOMs-)RO_2 compounds can be terminated with NO to form first generation nitrates (R 4.4); similarly, second generation (HOMs-)RO_2 form second generation nitrates upon NO termination (R 4.5).

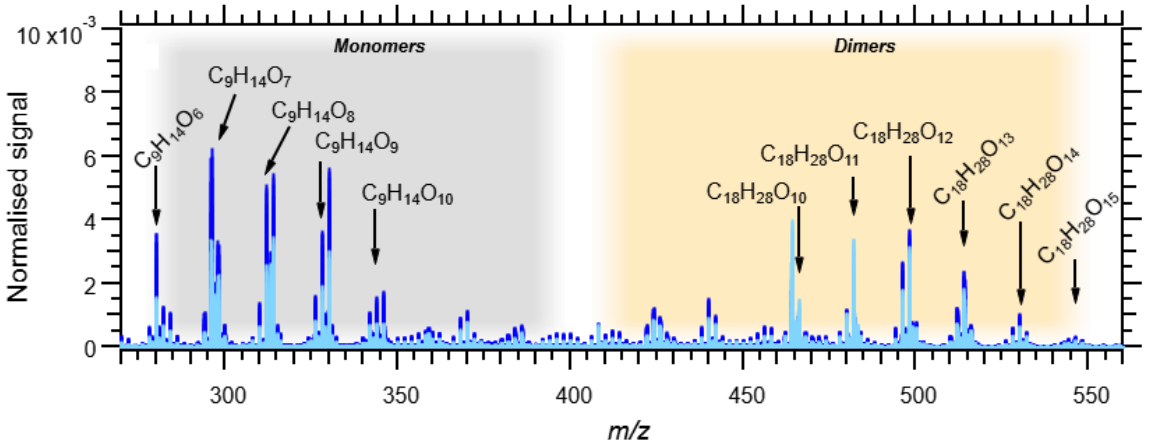

(a) Mass spectra of experiment 4 (dark blue) and experiment 3 (light blue). Dimer formation was reduced in experiment 1, which used the highest OH exposure, probably because of condensational loss to particles.

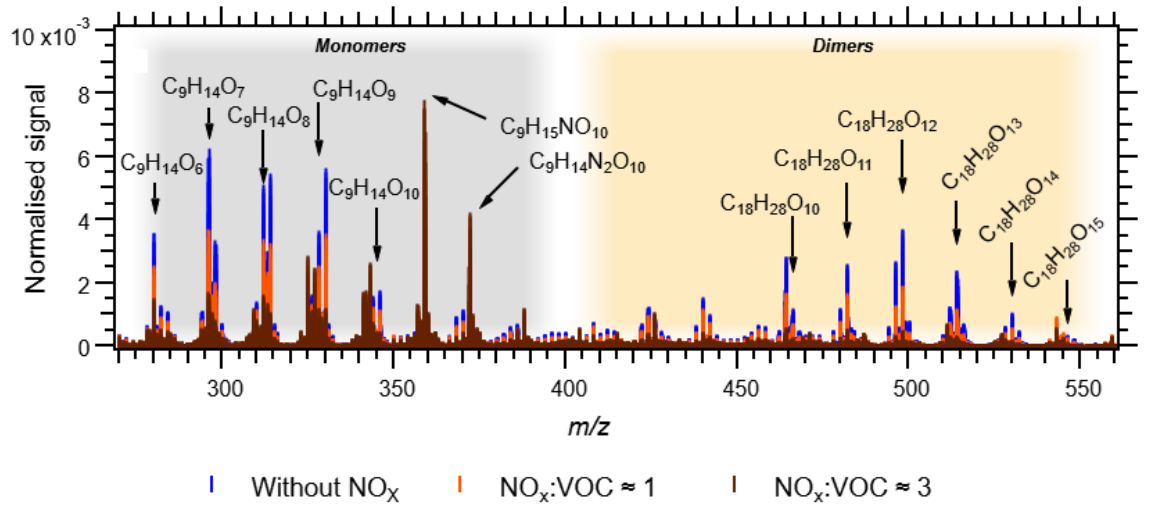

(b) Nitrate formation increased with the NO_x/VOC ratio, and dimer formation was suppressed. The dominant nitrates were $C_9H_{15}NO_{10}$ and $C_9H_{14}N_2O_{10}$.

Figure 4.4: Overview of the product distribution from OH-initiated TMB oxidation. Signals in the m/z ranges 270-330 and 450-560 are attributed to monomers (C9) and dimers (C18), respectively.Figure 4.4a shows results for experiments 3 and 4, while figure 4.4b shows results for experiments NO_x1_H and NO_x3_H.

$$C_9H_{13}O_{5-11}\bullet + NO \longrightarrow C_9H_{13}NO_{6-12} \quad \text{(R 4.4)}$$

$$C_9H_{15}O_{7-11}\bullet + NO \longrightarrow C_9H_{15}NO_{8-12} \quad \text{(R 4.5)}$$

The first generation nitrates, $C_9H_{13}NO_{7\text{-}8}$, were among the 10 most abundant compounds in experiments NO_x3_L and NO_x9. These ON can be formed from the radicals $C_9H_{13}O_6$ and $C_9H_{13}O_7$, respectively. The even oxygen number of $C_9H_{13}O_6$ indicates that the compound must have undergone a transformation to RO (via reaction with RO_2 or NO) and a subsequent H-shift followed by further O_2 addition [41]. The contributions of second generation nitrates increase with OH exposure because of the greater likelihood of second generation HOMs-RO_2 production. The RO_2 precursors of $C_9H_{15}O_{7\text{-}8}$ are probably species that underwent termination early in the radical chain process and so are not classified as HOMs (i.e. $C_9H_{14}O_{4\text{-}5}$). Second generation nitrates may form via the attack of OH on first generation nitrates if the radical chain is terminated via a (R 4.6) or hydroperoxyl (R 4.7) forming pathway:

$$C_9H_{14}NO_{8-12}\bullet + RO_2 \longrightarrow C_9H_{15}NO_{8-12} + R{=}O \quad \text{(R 4.6)}$$

$$C_9H_{14}NO_{8-12}\bullet + HO_2 \longrightarrow C_9H_{15}NO_{8-12} + O_2 \quad \text{(R 4.7)}$$

The formation of the most abundant dinitrates, which have the formula $C_9H_{14}N_2O_{8\text{-}12}$, must involve the attack of OH on a nitrated compound, $C_9H_{13}NO_{6\text{-}10}$, and termination of the RO_2 radical chain with NO (R 4.8

$$C_9H_{14}NO_{7-11}\bullet + NO \longrightarrow C_9H_{14}N_2O_{8-12} \quad \text{(R 4.8)}$$

The precursor species $C_9H_{14}NO_7$ would in this case be formed by the attack of OH on the smallest possible nitrate $C_9H_{13}NO_4$ (formed by NO termination after one auto-oxidation step). The formation of PAN-like compounds (R 2.6) cannot be ruled out as a nitrate formation mechanism, but is likely to require a stabilizing carbonyl group on the peroxy-bearing carbon.

The kinetic box model's predictions agreed well with the observed levels of bulk monomers, dimers, and ON. We successfully described the system's general behaviour using the dimer formation rate coefficient of $2{*}10^{-12}$ $cm^3molecules^{-1}s^{-1}$ proposed by Zhao *et al.* [88], which is two orders of magnitude smaller than that suggested by Berndt *et al.* [87]. The formation of monomer species or RO from the RO_2 self-reaction was modeled using an assumed rate constant of $1{*}10^{-12}$ $cm^3molecules^{-1}s^{-1}$.

4.5 GUFIT and VP estimates

During the work on Paper III, it was discovered that FIGAERO thermograms can be rather challenging to analyse. These thermograms may feature multiple peaks; in such cases, it is assumed that the first peak corresponds to the compound evaporating from the filter and subsequent peaks are due to fragments of thermally unstable oligomers, as discussed in Paper II. Single thermograms can be evaluated manually to determine T_{Max}, but such assessments are impractical when dealing with large datasets based on time series or when many compounds are to be investigated (as is the norm when analysing complex aerosols). These problems were overcome by developing the GUFIT algorithm, which automatically extracts peak areas and T_{Max} values from (multipeak) FIGAERO thermograms (see figure 4.5). This algorithm was developed while evaluating the data presented in Paper III and is discussed further in Paper V

GUFIT was written in Python 3.6.0 using the NumPy (v 1.11.3), SciPy (v 0.19.1), lmfit (0.9.6) and pandas (v 0.19.2) libraries. Thermogram data are loaded into Python and corrected to account for the flow difference between sampling on the filter (4lpm) and desorption from the filter (2lpm). Estimated T_{Max} values used as the initial parameters in the fit function are calculated by finding minima in the slope of the thermogram. The exponentially modified Gaussian (EMG, equation 4.1) [91, 92], a Gaussian function convoluted with an exponential decay function, is used as the single peak shape for the model:

$$f(x) = \frac{A}{2\tau} exp\left[\left(\frac{W}{2\tau}\right)^2 + \frac{T-x}{\tau}\right]\left[erf\left(\frac{x-T}{\sqrt{2}W} - \frac{W}{\sqrt{2}\tau}\right) + 1\right] \tag{4.1}$$

Here, A is the area, T is T_{Max}, W the width of the Gaussian, τ the exponential damping term, and erf is the error function. The initial guesses were empirically determined for the 3 terms A (equation 4.2), W (equation 4.3) and τ (equation 4.4) and were calculated from T_{Max} and the signal intensity H at T_{Max} :

$$A = \frac{H\sqrt{W}}{0.3989} \tag{4.2}$$

$$W = \frac{T_{Max}}{2} \tag{4.3}$$

$$\tau = T_{Max} \tag{4.4}$$

The following, empirically determined, constraints were set for the parameters for EMG 1, 2 and 3:

EMG1 A1: min = 0.0001, max = inf; T1: min = T_{Max1} - 10, max = T_{Max1} + 3; W1: min = 0, max = 30; τ1: min = 0, max = inf test
EMG2 A2: min = 0.00001, max = inf; T2: min = T_{Max2} - 3, max = T_{Max2} + 20; W2, min = 5, max = 30; τ2, min = 0, max = inf
EMG3 A3: min = 0, max = inf; T3: min = T_{Max3}, max = T_{Max3} + 20; W3, min = 0, max = inf; τ3, min = 0, max = inf

To accurately model the shape of a thermogram, two to three EMG were convoluted. The lmfit package for Python [93] was used to fit the convoluted EMG model to real thermogram data by minimizing the residual function. Equation 4.5 shows the residual function with a model of three convoluted EMG:

$$res = (EMG1 + EMG2 + EMG3) - data \tag{4.5}$$

The following fitting methods and smoothing parameters were compared to find the best fit of the Gaussian model to the data:

Fit methods:	leastsq, nelder, powell
Window types for smoothing:	flat, hanning, hamming, bartlett, blackman
Window lengths for smoothing:	1, 3, 5, 7, 9, 11, 13, 15

The combination with the lowest residual was chosen as the final fit. If the sum of the residual was larger than 15% of the sum of the signals of peak 1, the fitting process was repeated using the sciPy.curve_fit function. If the sciPy fit gave a larger residual than lmfit, the lmfit was chosen (see figure 4.5). By extracting information on T_{Max} and peak area from FIGAERO thermograms, specific compounds can be quantified if compared to a standard and information on their VP can be estimated as described in Paper V.

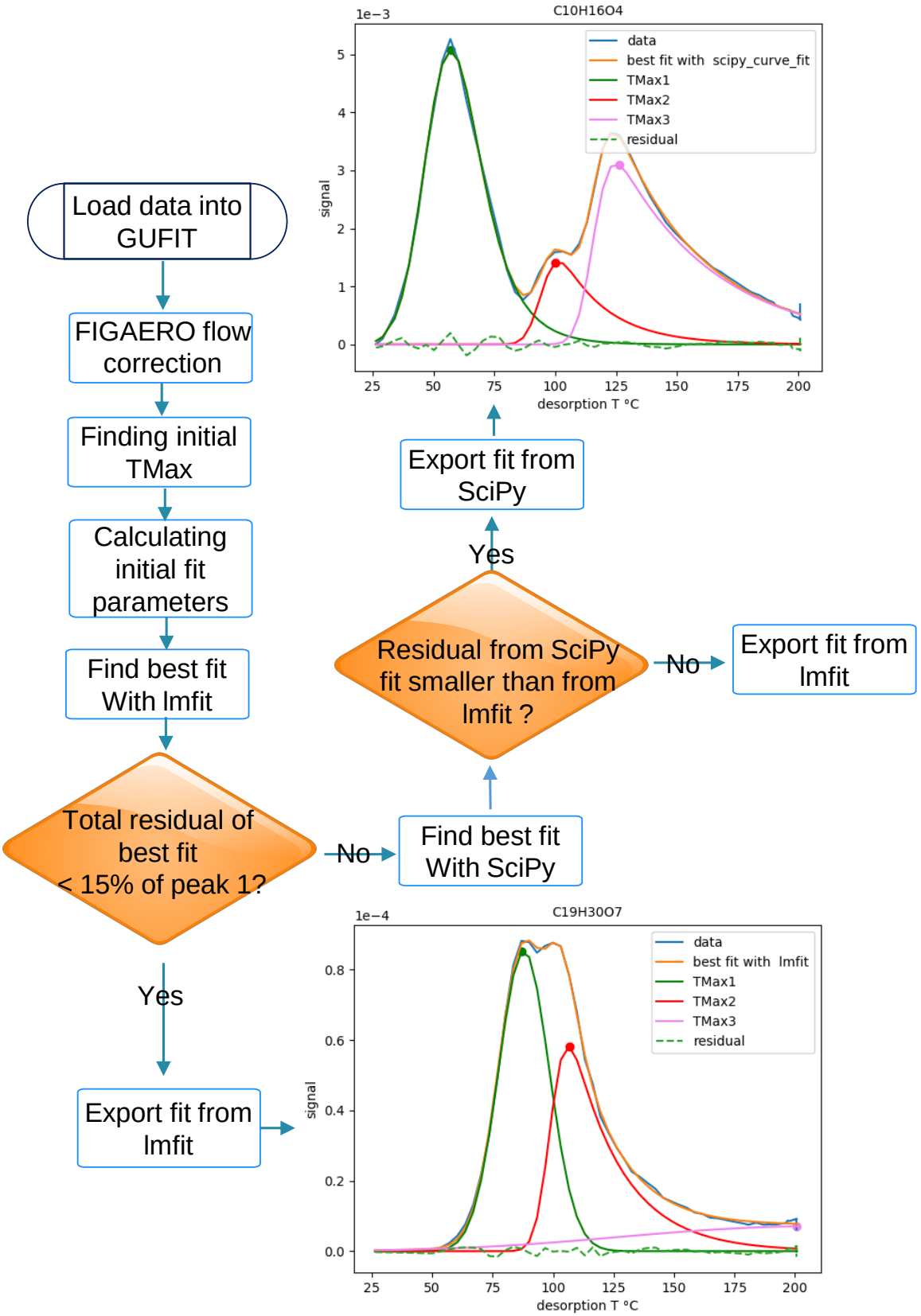

Figure 4.5: Work flow of the GUFIT algorithm with two illustrative fits generated using lmfit and scipy methods. Data from Paper III and illustration adapted from Paper V.

Paper V presents a method for extracting volatility data from FIGAERO thermograms. A series of homologous polyethylene glycols (PEG) with known VP, spanning the atmospherically relevant range of $10^{-1} - 10^{-7} Pa$, was analysed with the FIGAERO-CIMS and their T_{Max} values were extracted from the thermograms. Plotting the known VP of PEG versus their T_{Max} and fitting an exponential function to the data, the follwing relationship could be established:

$$VP(Pa) = 0.2612 exp\left(- 0.071 T_{Max} \right) \tag{4.6}$$

To evaluate the goodness of the VP calibration function (4.6), it was tested against a series of 7 pure dicarboxylic acids with known VP [14]. The VP values calculated for these acids using the new method were in good agreement with the literature values. It should be noted that the VP is defined for a pure system that is in thermodynamic phase equilibrium and contains only the compound of interest, but atmospheric aerosols are mixed systems with many components and are not in equilibrium. To determine whether equation 4.6 also holds for complex mixtures, SOA was generated from α-pinene + O_3 in the Manchester Photochemical Aerosol Chamber, and T_{Max} values for 6 acids were extracted. Their VP values were calculated and found to agree well with literature values. The selected PEG compounds thus proved to be useful calibrants for atmospherically relevant VP ranges and may enable the extraction of VP data for as-yet uncharacterized aerosol constituents. Additionally, while the results obtained with the FIGAERO-CIMS instruments in Manchester and Gothenburg are in good agreement, each FIGAERO unit must be calibrated individually to account for potential differences in construction and design (for example, differences in the locations of thermocouples) that may affect the shape of the thermograms. Additionally, VP calibration must be performed using the same temperature ramping profile as the actual measurements.

5

Concluding remarks, atmospheric implications and future perspectives

This chapter summarizes and concludes the dissertation, and links the results of the experimental studies to the real world. Implications for indoor and outdoor environments are addressed and suggestions for future studies are offered.

This work characterizes the formation of highly functionalized oxidation products from α-pinene, limonene, and TMB, all of which are known to be important contributors to SOA formation. One group of molecules previously identified as ELVOCs are dimers, which were detected as products from all three precursor molecules (α-pinene, limonene and TMB). Multiple mechanisms for the formation of oxidation products have been identified.

Notably, the process leading to dimer formation during the ozonolysis of α-pinene and limonene is suggested to involve the reaction of a sCI with a carboxylic acid. This theory is supported by the absence of dimer products during the OH-initiated oxidation of α-pinene and the weak signal of acidic dimers during limonene ozonolysis.

A wide range of nitrated products that contribute to SOA formation were detected during nitrate-initiated limonene oxidation. Dimers are known to be abundant in the particle phase, and dimerization has been suggested to occur via a condensation process in which HNO_3 acts as the leaving group. The low O/C ratio of dimers compared to monomers supports this theory. Many of the nitrated compounds observed in this work were previously unknown, and the formation of dinitrated species suggests that secondary chemistry occurs following the initial addition of nitrate to the endocyclic double bond of limonene. These results clearly show that nocturnal limonene chemistry contributes to SOA formation.

Carboxylic and dicarboxylic acids were produced in large amounts during limonene ozonolysis. They were found in both the gas and particle phases, and contributed to SOA formation. In addition, the formation of acidic dimers which were found almost exclusively in the particle phase was observed. Explicit reaction mechanisms were proposed to explain the formation of these previously unknown compounds.

Particle formation from TMB oxidation was observed and linked to the formation of HOMs monomers and dimers. SOA formation was significantly reduced in the presence of NO_x, and the oxidation product distribution shifted from HOMs to ON, with dimers being affected particularly strongly. The suppression of HOMs formation was attributed to the reaction of HOMs-RO_2 with NO_x and the subsequent formation of ONs that are too volatile to initiate NPF.

All results presented here were obtained in a controlled laboratory environment. Consequently, one cannot assume that they will carry over directly to the real atmosphere. Rather, they provide a link between simplified models and the real world [94]. SOA has a cooling effect on the climate, and to correctly assess its influence, climate models must be fed with reliable SOA estimates [4].

One way to improve these estimates is to improve our understanding of the underlying chemistry and physical properties, which was the aim of this work.
SOA is a major component of urban air pollution [5–9] and the AVOCs contributing to air pollution are often oxidised in the presence of NO_x. Although studies in NO_x free environments have demonstrated the formation of ELVOCs from AVOC oxidation [62, 63] and subsequent NPF, we conclude that the presence of NO_x can prevent NPF by preventing ELVOC formation. The produced ON may contribute to condensational growth of pre-existing particles but not to NPF.
While terpene emissions dominate the VOC budget in rural and remote regions [24, 25], terpenes are also found at elevated levels indoors, where humans living in first world countries spent most of their lifetime [26, 27]. The results of this work suggest that VOC oxidation generates a wide variety of low volatility compounds and that elevated SOA levels can be expected indoors, potentially posing a risk to human health.

The work done in this thesis shows that much remains to be learned about the fundamental molecular processes of atmospheric chemistry and SOA formation. The generally higher complexity of the particle phase formed during limonene ozonolysis hints at condensed phase reactions, which remain poorly characterized. Further research is needed because the chemical composition and properties of the particle phase cannot be defined solely by studying the partitioning of gas phase species. The work presented here opens up several ways to better understand VOC oxidation and SOA formation. For example, to gain a more complete picture of the product distribution from VOC oxidation, aerosols could be analysed using multiple ionisation schemes simultaneously.

To conclude, this dissertation enhances our fundamental understanding of VOC oxidation mechanisms and the formation of low volatility oxidation products. State of the art methodologies and scientific instruments, i.e. FIGAERO - CIMS, were used to elucidate the oxidation product distribution in VOC-derived aerosol. Knowledge of the specific molecular formulas of the oxidation products and the way they change in response to variation in experimental parameters made it possible to propose explicit mechanisms for their formation. In addition, improved data evaluation methods were developed during this work, culminating in the development of the GUFIT algorithm for compound quantification and extraction of volatility information from FIGAERO thermograms.

Acknowledgements

Rome wasn't built in a day and it surely was not built by one person alone!
This thesis would not have been possible without the continuous encouragement and support of many wonderful people.
Firstly, I would like to express my sincere gratitude to my supervisor Professor Mattias Hallquist for support, patience, motivation and immense knowledge. I would like to thank my co-supervisor PD Dr. Thomas Mentel for insightful comments, encouragement and giving me the possibility to work with the nitrate CIMS. Professor Johan Boman has been a supportive and encouraging examiner during those years and I especially want to thank him for always having a smile and kind words for me. I would like to thank all co-authors and peer reviewers for investing their time and giving valuable comments and questions. My research was funded by the strategic swedish research area MERGE (ModElling the Regional and Global Earth system) and supported by the Swedish Research Council (grant number 2014-5332) and Formas (grant number 2015-1537). Adlerbertska Stipendiestiftelsen, Knut och Alice Wallenbergs Stiftelse, Paul och Marie Berghaus donationsfond and Åforsk are acknowledged for generous travel grants. All this could not have been done without using open source software. I want to give special thanks to all developers out there that invest their passion and time into making these tools available to all of us.
Coffee ☕ and a good support system 🧍🧍🧍 are essential for surviving and staying sane during the PhD. I want to thank Professor Anna Wåhlin, for always having an open ear for me. I am glad to have you as my mentor and friend and our lunch meeting gave me insight and perspective of the academic world, and that professors are also just humans ☺. The whole atmospheric science group with its current and former members deserves a special thank you for providing a friendly and warm working atmosphere [pun intended]. I especially want to thank the atmochicks Anna L., Sofia J. and Ågot W. for laughter, nonsense, common sense, bubbel and scientific and mental support. It feels good to be part of a ladies group in a male dominated environment! Nondas T., thank you for being a great lab partner and co-author! Thank you Dan G. and Mike LB. for being awesome office mates and discussion partners and Mwaniki "Sam" G. and Christian S. for fun board game nights and fotos. Finally I would like to thank my parents and my brother for always being there for me, supporting me and believing in me! ♡

Bibliography

[1] New York State Education Department. *Physical Setting/Earth Science Reference Tables — 2011 Edition*. 2011.

[2] B. J. Finlayson-Pitts et al. *Chemistry of the Upper and Lower Atmosphere*. 2000.

[3] European Environment Agency. *Air quality in Europe — 2018 report*. Tech. rep. 2018.

[4] IPCC. *Climate Change 2013: The Physical Science Basis. Contribution of Working Group I to the Fifth Assessment Report of the Intergovernmental Panel on Climate Change*. Cambridge, United Kingdom and New York, NY, USA: Cambridge University Press, 2013.

[5] M. Hallquist et al. "The formation, properties and impact of secondary organic aerosol: current and emerging issues". In: *Atmospheric Chem. Phys.* 9.14 (2009), pp. 5155–5236.

[6] C. K. Chan et al. "Air pollution in mega cities in China". In: *Atmos. Env.* 42.1 (2008), pp. 1–42.

[7] M. Hu et al. "Insight into characteristics and sources of PM2.5 in the Beijing–Tianjin–Hebei region, China". In: *Natl. Sci. Rev.* 2.3 (2014), pp. 257–258.

[8] S. Guo et al. "Elucidating severe urban haze formation in China". In: *Proc. Natl. Acad. Sci. U.S.A* 111.49 (2014), pp. 17373–17378.

[9] M. Hallquist et al. "Photochemical smog in China: scientific challenges and implications for air-quality policies". In: *Natl. Sci. Rev.* 3.4 (2016), pp. 401–403.

[10] F. Yasmeen et al. "Terpenylic acid and related compounds: precursors for dimers in secondary organic aerosol from the ozonolysis of alpha- and beta-pinene". In: *Atmospheric Chem. Phys.* 10.19 (2010), pp. 9383–9392.

[11] K. Kristensen et al. "Formation and occurrence of dimer esters of alpha-pinene oxidation products in atmospheric aerosols". In: *Atmospheric Chem. Phys. Discuss.* 12.8 (2012), pp. 22103–22137.

[12] K. Salo et al. "Aerosol volatility and enthalpy of sublimation of carboxylic acids". In: *J. Phys. Chem. A* 114.13 (2010), pp. 4586–4594.

[13] R. K. Pathak et al. “Influence of ozone and radical chemistry on limonene organic aerosol production and thermal characteristics”. In: *Environ. Sci. Technol.* 46.21 (2012), pp. 11660–11669.

[14] M. Bilde et al. “Saturation Vapor Pressures and Transition Enthalpies of Low-Volatility Organic Molecules of Atmospheric Relevance: From Dicarboxylic Acids to Complex Mixtures”. In: *Natl. Sci. Rev.* 115.10 (2015), pp. 4115–4156.

[15] S. S. Brown et al. “Nighttime radical observations and chemistry”. In: *Chem. Soc. Rev.* 41.19 (2012), pp. 6405–6547.

[16] N. L. Ng et al. “Nitrate radicals and biogenic volatile organic compounds: oxidation, mechanisms, and organic aerosol”. In: *Atmospheric Chem. Phys.* 17.3 (2017), pp. 2103–2162.

[17] M. Ehn et al. “Gas phase formation of extremely oxidized pinene reaction products in chamber and ambient air”. In: *Atmospheric Chem. Phys.* 12.11 (2012), pp. 5113–5127.

[18] M. Ehn et al. “A large source of low-volatility secondary organic aerosol”. In: *Nature* 506.7489 (2014), pp. 476–479.

[19] C. Mohr et al. “Ambient observations of dimers from terpene oxidation in the gas phase: Implications for new particle formation and growth”. In: *Geophys. Res. Lett.* 44.6 (2017), pp. 2958–2966.

[20] V.-M. Kerminen et al. “Atmospheric new particle formation and growth: review of field observations”. In: *Environ. Res. Lett.* 13.10 (2018), pp. 103003–103041.

[21] F. Bianchi et al. “New particle formation in the free troposphere: A question of chemistry and timing”. In: *Science* 352.6289 (2016), pp. 1109–1112.

[22] J. H. Seinfeld et al. *Atmospheric chemsitry and physics. From air pollution to climate change*. 2006.

[23] J. L. Jimenez et al. “Evolution of organic aerosols in the atmosphere”. In: *Science* 326.5959 (2009), pp. 1525–1529.

[24] P. J. Ziemann et al. “Kinetics, products, and mechanisms of secondary organic aerosol formation”. In: *Chem. Soc. Rev.* 41.19 (2012), pp. 6582–6605.

[25] H. Hakola et al. “In situ measurements of volatile organic compounds in a boreal forest”. In: *Atmospheric Chem. Phys.* 12.23 (2012), pp. 11665–11678.

[26] S. K. Brown et al. “Concentrations of Volatile Organic-Compounds in Indoor Air - a Review”. In: *Indoor Air* 4.2 (1994), pp. 123–134.

[27] S. Langer et al. “Ultrafine particles produced by ozone/limonene reactions in indoor air under low/closed ventilation conditions”. In: *Atmos. Env.* 42.18 (2008), pp. 4149–4159.

[28] D. V. Spracklen et al. “Aerosol mass spectrometer constraint on the global secondary organic aerosol budget”. In: *Atmospheric Chem. Phys.* 11.23 (2011), pp. 12109–12136.

[29] J. F. Pankow. “An absorption model of the gas/aerosol partitioning involved in the formation of secondary organic aerosol”. In: *Atmos. Env.* 28.2 (1994), pp. 189–193.

[30] K. C. Barsanti et al. “Analyzing experimental data and model parameters: implications for predictions of SOA using chemical transport models”. In: *Atmospheric Chem. Phys.* 13.23 (2013), pp. 12073–12088.

[31] J. Li et al. “Modeling regional secondary organic aerosol using the Master Chemical Mechanism”. In: *Atmos. Env.* 102 (2015), pp. 52–61.

[32] M. E. Jenkin. “Modelling the formation and composition of secondary organic aerosol from alpha- and beta-pinene ozonolysis using MCM v3”. In: *Atmospheric Chem. Phys.* 4.7 (2004), pp. 1741–1757.

[33] R. Volkamer et al. “Secondary organic aerosol formation from anthropogenic air pollution: Rapid and higher than expected”. In: *Geophys. Res. Lett.* 33.17 (2006), pp. 1–4.

[34] S. R. Utembe et al. “Simulating secondary organic aerosol in a 3-D Lagrangian chemistry transport model using the reduced Common Representative Intermediates mechanism (CRI v2-R5)”. In: *Atmos. Env.* 45.8 (2011), pp. 1604–1614.

[35] M. Kulmala et al. “Direct observations of atmospheric aerosol nucleation”. In: *Science* 339.6122 (2013), pp. 943–646.

[36] R. Zhang et al. “Nucleation and growth of nanoparticles in the atmosphere”. In: *Chem. Rev.* 112.3 (2012), pp. 1957–2011.

[37] I. Riipinen et al. “The contribution of organics to atmospheric nanoparticle growth”. In: *Nat. Geosci.* 5.7 (2012), pp. 453–458.

[38] N. M. Donahue et al. “A two-dimensional volatility basis set – Part 2: Diagnostics of organic-aerosol evolution”. In: *Atmospheric Chem. Phys.* 12.2 (2012), pp. 615–634.

[39] J. D. Crounse et al. “Autoxidation of Organic Compounds in the Atmosphere”. In: *J. Phys. Chem. Lett* 4.20 (2013), pp. 3513–3520.

[40] T. Jokinen et al. “Production of extremely low volatile organic compounds from biogenic emissions: Measured yields and atmospheric implications”. In: *Proc. Natl. Acad. Sci. U.S.A* 112.23 (2015), pp. 7123–7128.

[41] T. F. Mentel et al. “Formation of highly oxidized multifunctional compounds: autoxidation of peroxy radicals formed in the ozonolysis of alkenes – deduced from structure–product relationships”. In: *Atmospheric Chem. Phys.* 15.12 (2015), pp. 6745–6765.

[42] T. Berndt et al. “Hydroxyl radical-induced formation of highly oxidized organic compounds”. In: *Nat. Commun.* 7 (2016), pp. 13677–13685.

[43] J. Trostl et al. “The role of low-volatility organic compounds in initial particle growth in the atmosphere”. In: *Nature* 533.7604 (2016), pp. 527–531.

[44] T. Kurten et al. “Alpha-Pinene Autoxidation Products May Not Have Extremely Low Saturation Vapor Pressures Despite High O/C Ratios”. In: *J. Phys. Chem. A* 120.16 (2016), pp. 2569–2582.

[45] I. Riipinen et al. “The contribution of organics to atmospheric nanoparticle growth”. In: *Nat. Geosci* 5.7 (2012), pp. 453–458.

[46] N. M. Donahue et al. “Theoretical constraints on pure vapor-pressure driven condensation of organics to ultrafine particles”. In: *Geophys. Res. Lett.* 38.16 (2011), pp. 1–5.

[47] J. Zhao et al. “Dependence of particle nucleation and growth on high-molecular-weight gas-phase products during ozonolysis of alpha-pinene”. In: *Atmospheric Chem. Phys.* 13.15 (2013), pp. 7631–7644.

[48] J. Kirkby et al. “Ion-induced nucleation of pure biogenic particles”. In: *Nature* 533.7604 (2016), pp. 521–526.

[49] R. Atkinson et al. “Gas-phase tropospheric chemistry of biogenic volatile organic compounds: a review”. In: *Atmos. Env.* 37 (2003), pp. 197–219.

[50] C. T. Pate et al. “The gas phase reaction of ozone with a series of aromatic hydrocarbons”. In: *Journal of Environmental Science and Health . Part A: Environmental Science and Engineering* 11.1 (1976), pp. 1–10.

[51] C. Bloss et al. “Development of a detailed chemical mechanism (MCMv3.1) for the atmospheric oxidation of aromatic hydrocarbons”. In: *Atmospheric Chem. Phys.* 5.3 (2005), pp. 641–664.

[52] C. S. Maksymiuk et al. “Secondary organic aerosol formation from multiphase oxidation of limonene by ozone: mechanistic constraints via two-dimensional heteronuclear NMR spectroscopy”. In: *Phys. Chem. Chem. Phys.* 11.36 (2009), pp. 7810–7818.

[53] L. Vereecken et al. “Theoretical studies of atmospheric reaction mechanisms in the troposphere”. In: *Chem. Soc. Rev.* 41.19 (2012), pp. 6259–6293.

[54] A. R. Rickard et al. “OH Yields in the Gas-Phase Reactions of Ozone with Alkenes”. In: *J. Phys. Chem. A* 103.38 (1999), pp. 7656–7664.

[55] J. G. Calvert et al. *The Mechanisms of Atmospheric Oxidation of the Alkenes*. 2000.

[56] K. Kristensen et al. “High-Molecular Weight Dimer Esters Are Major Products in Aerosols from alpha - Pinene Ozonolysis and the Boreal Forest”. In: *Environ. Sci. Technol. Lett.* 3.8 (2016), pp. 280–285.

[57] S. Lee et al. “Particle nucleation from the reaction of alpha-pinene and ozone”. In: *Atmos. Env.* 39.36 (2005), pp. 6822–6832.

[58] B. Witkowski et al. “Early stage composition of SOA produced by alpha-pinene/ozone reaction: alpha-Acyloxyhydroperoxy aldehydes and acidic dimers”. In: *Atmos. Env.* 95 (2014), pp. 59–70.

[59] M. Wang et al. “Reactions of Atmospheric Particulate Stabilized Criegee Intermediates Lead to High-Molecular-Weight Aerosol Components”. In: *Environ. Sci. Technol.* 50.11 (2016), pp. 5702–5710.

[60] J. Zhang et al. “Continuous measurement of peroxyacetyl nitrate (PAN) in suburban and remote areas of western China”. In: *Atmos. Env.* 43.2 (2009), pp. 228–237.

[61] K. C. Barsanti et al. “Formation of Low-Volatility Organic Compounds in the Atmosphere: Recent Advancements and Insights”. In: *J. Phys. Chem. Lett* 8.7 (2017), pp. 1503–1511.

[62] U. Molteni et al. “Formation of highly oxygenated organic molecules from aromatic compounds”. In: *Atmospheric Chem. Phys.* 18.3 (2018), pp. 1909–1921.

[63] S. Wang et al. “Formation of Highly Oxidized Radicals and Multifunctional Products from the Atmospheric Oxidation of Alkylbenzenes”. In: *Environ. Sci. Technol.* 51.15 (2017), pp. 8442–8449.

[64] MCM. *Master Chemical Mechanism, MCM v3.3.1.* http://mcm.leeds.ac.uk/MCM. 2018.

[65] A. M. Jonsson et al. "Influence of OH Scavenger on the Water Effect on Secondary Organic Aerosol Formation from Ozonolysis of Limonene, delta3-Carene, and alpha-pinene". In: *Environ. Sci. Technol.* 42.16 (2008), pp. 5938–5944.

[66] E. Kang et al. "Introducing the concept of Potential Aerosol Mass (PAM)". In: *Atmospheric Chem. Phys.* 7.22 (2007), pp. 5727–5744.

[67] A. K. Watne et al. "Fresh and Oxidized Emissions from In-Use Transit Buses Running on Diesel, Biodiesel, and CNG". In: *Environ. Sci. Technol.* 52.14 (2018), pp. 7720–7728.

[68] P. Veres et al. "Development of negative-ion proton-transfer chemical-ionization mass spectrometry (NI-PT-CIMS) for the measurement of gas-phase organic acids in the atmosphere". In: *IJMS* 274.1-3 (2008), pp. 48–55.

[69] D. Aljawhary et al. "High-resolution chemical ionization mass spectrometry (ToF-CIMS): application to study SOA composition and processing". In: *Atmospheric Meas. Tech.* 6.11 (2013), pp. 3211–3224.

[70] H. Junninen et al. "A high-resolution mass spectrometer to measure atmospheric ion composition". In: *Atmospheric Meas. Tech.* 3.4 (2010), pp. 1039–1053.

[71] F. L. Eisele et al. "Measurement of the gas phase concentration of sulfuric acid and methane sulfonic acid and estimates of sulfuric acid production and loss in the atmosphere". In: *JGR: Atmospheres* 98.D5 (1993), pp. 9001–9010.

[72] T. H. Bertram et al. "A field-deployable, chemical ionization time-of-flight mass spectrometer". In: *Atmospheric Meas. Tech.* 4.7 (2011), pp. 1471–1479.

[73] F. D. Lopez-Hilfiker et al. "A novel method for online analysis of gas and particle composition: description and evaluation of a Filter Inlet for Gases and AEROsols (FIGAERO)". In: *Atmospheric Meas. Tech.* 7.4 (2014), pp. 983–1001.

[74] X. Zhang et al. "Highly Oxygenated Multifunctional Compounds in alpha-pinene Secondary Organic Aerosol". In: *Environ. Sci. Technol.* 51.11 (2017), pp. 5932–5940.

[75] X. Zhang et al. "Formation and evolution of molecular products in alpha-pinene secondary organic aerosol". In: *Proc. Natl. Acad. Sci. U.S.A* 112.46 (2015), pp. 14168–14173.

[76] T. Nah et al. “Photochemical Aging of alpha-pinene and beta-pinene Secondary Organic Aerosol formed from Nitrate Radical Oxidation”. In: *Environ. Sci. Technol.* 50.1 (2016), pp. 222–231.

[77] B. H. Lee et al. “Highly functionalized organic nitrates in the southeast United States: Contribution to secondary organic aerosol and reactive nitrogen budgets”. In: *Proc. Natl. Acad. Sci. U.S.A* 113.6 (2016), pp. 1516–1521.

[78] A. M. Jonsson et al. “Impact of Humidity on the Ozone Initiated Oxidation of Limonene, delta3-Carene, and alpha-pinene”. In: *Environ. Sci. Technol.* 40.1 (2005), pp. 188–194.

[79] S. Leungsakul et al. “A kinetic mechanism for predicting secondary aerosol formation from the reactions of d-limonene in the presence of oxides of nitrogen and natural sunlight”. In: *Atmos. Env.* 39.37 (2005), pp. 7063–7082.

[80] M. L. Walser et al. “High-resolution mass spectrometric analysis of secondary organic aerosol produced by ozonation of limonene”. In: *Phys. Chem. Chem. Phys.* 10.7 (2008), pp. 1009–1022.

[81] M. Jaoui et al. “Identification and quantification of aerosol polar oxygenated compounds bearing carboxylic or hydroxyl groups. 2. Organic tracer compounds from monoterpenes”. In: *Environ. Sci. Technol.* 39.15 (2005), pp. 5661–5673.

[82] M. Jaoui et al. “Analysis of Secondary Organic Aerosol Compounds from the Photooxidation of d-Limonene in the Presence of NOx and their Detection in Ambient PM2.5”. In: *Environ. Sci. Technol.* 40.12 (2006), pp. 3819–3828.

[83] S. Rossignol et al. “The use of a housecleaning product in an indoor environment leading to oxygenated polar compounds and SOA formation: Gas and particulate phase chemical characterization”. In: *Atmos. Env.* 75 (2013), pp. 196–205.

[84] M. Glasius et al. “Carboxylic Acids in Secondary Aerosols from Oxidation of Cyclic Monoterpenes by Ozone”. In: *Environ. Sci. Technol.* 34.6 (2000), pp. 1001–1010.

[85] L. Ran et al. “Ozone photochemical production in urban Shanghai, China: Analysis based on ground level observations”. In: *JGR: Atmospheres* 114.D15301 (2009), pp. 1–14.

[86] M. E. Jenkin et al. “Protocol for the development of the Master Chemical Mechanism, MCM v3 (Part B): tropospheric degradation of aromatic volatile organic compounds”. In: *Atmospheric Chem. Phys.* 3.1 (2003), pp. 181–193.

[87] T. Berndt et al. “Accretion Product Formation from Self- and Cross-Reactions of RO2 Radicals in the Atmosphere”. In: *Angew. Chem. Int. Ed.* 57.14 (2018), pp. 3820–3824.

[88] Y. Zhao et al. “Quantitative constraints on autoxidation and dimer formation from direct probing of monoterpene-derived peroxy radical chemistry”. In: *Proc. Natl. Acad. Sci. U.S.A* 15.48 (2018), pp. 12142–12147.

[89] T. Jokinen et al. “Rapid autoxidation forms highly oxidized RO2 radicals in the atmosphere”. In: *Angew. Chem. Int. Ed.* 53.52 (2014), pp. 14596–600.

[90] M. P. Rissanen et al. “The formation of highly oxidized multifunctional products in the ozonolysis of cyclohexene”. In: *J. Am. Chem. S* 136.44 (2014), pp. 15596–15606.

[91] M. S. Jeansonne et al. “Review of the Exponentially Modified Gaussian (Emg) Function since 1983”. In: *JCS* 29.6 (1991), pp. 258–266.

[92] K. J. Goodman et al. “Curve fitting for restoration of accuracy for overlapping peaks in gas chromatography/combustion isotope ratio mass spectrometry”. In: *Anal. Chem.* 66.8 (1994), pp. 1294–1301.

[93] M. Newville et al. *LMFIT: Non-Linear Least-Square Minimization and Curve-Fitting for Python*. 2014.

[94] J. B. Burkholder et al. “The Essential Role for Laboratory Studies in Atmospheric Chemistry”. In: *Environ. Sci. Technol.* 51.5 (2017), pp. 2519–2528.